Volume 5
Number 1
January 2026
Pages 1–294

Environmental Science Advances

rsc.li/esadvances

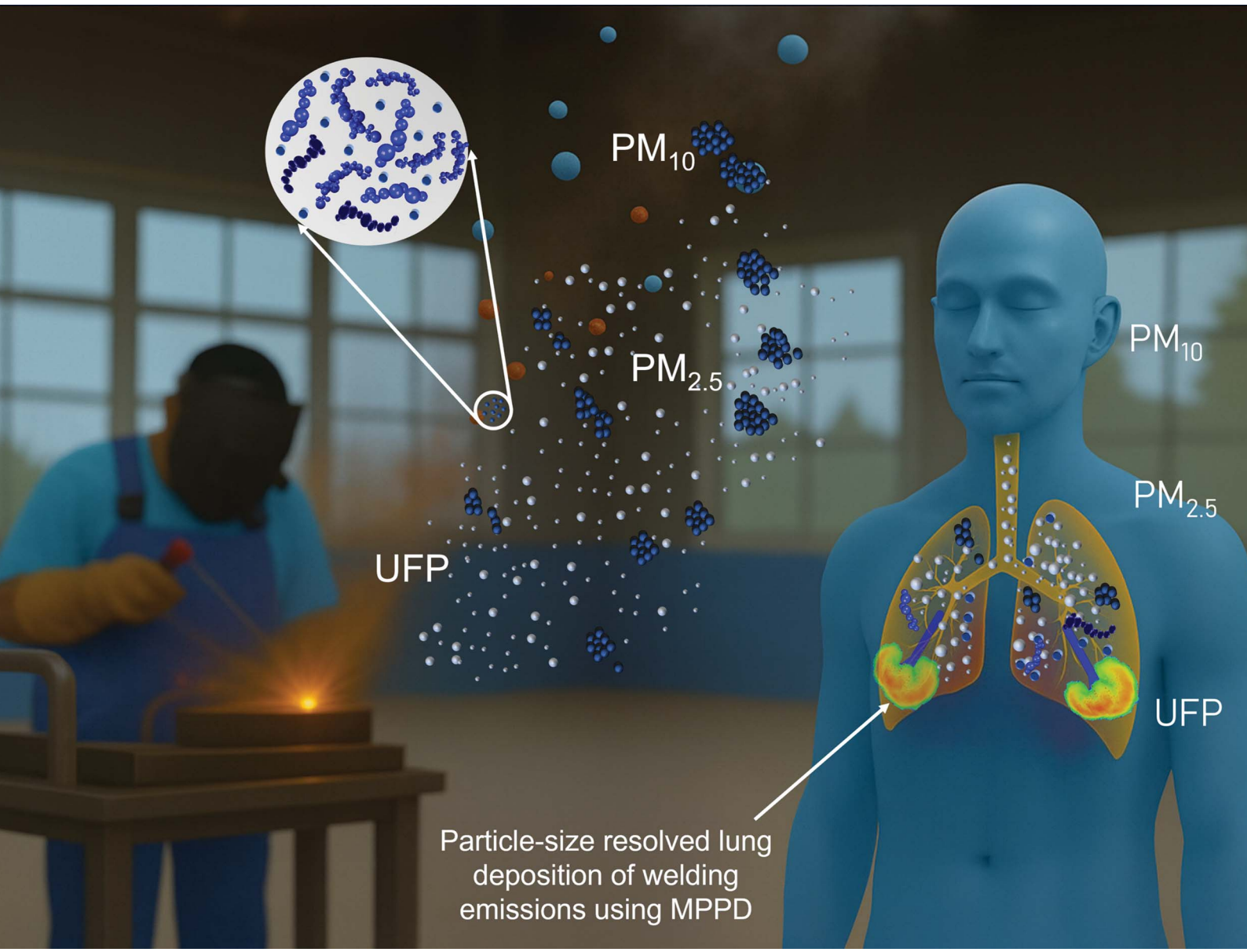

ISSN 2754-7000

ROYAL SOCIETY OF CHEMISTRY

PAPER

Rubal Dhiman, Thaseem Thajudeen *et al.*

Occupational health risks from welding emissions: exposure and deposition of PM_{10}, $PM_{2.5}$, and ultrafine particles across welding methods

Environmental Science Advances

ROYAL SOCIETY OF CHEMISTRY

PAPER

View Article Online
View Journal | View Issue

Cite this: *Environ. Sci.: Adv.*, 2026, **5**, 59

Occupational health risks from welding emissions: exposure and deposition of PM_{10}, $PM_{2.5}$, and ultrafine particles across welding methods

Rubal Dhiman,[a] Adarsh Prakash,[a] Subhrajyoti Saroj,[a] Priyabrata Sahoo,[a] Anirudha Ambekar,[ac] Sachin D. Kore,[a] Thaseem Thajudeen *[abc] and Sarath K. Guttikunda [d]

Welding emits high levels of particulate matter (PM) and ultrafine particles (UFPs), which are associated with health risks including asthma, chronic obstructive pulmonary disease (COPD), and certain cancers. This study quantifies inhalation doses and health risks from different PM size fractions (PM_{10}, $PM_{2.5}$, and UFPs: 15–595 nm) generated by Shielded Metal Arc Welding (SMAW), Wire Arc Additive Manufacturing (WAAM), and Friction Stir Welding (FSW) under typical industrial conditions. Real-time PM and UFP concentrations were measured using a scanning-mobility-particle-sizer and low-cost PM sensors. Inhalation doses were estimated based on age, height, breathing frequency, inhalation rate, activity levels, and density variation (2 to 7 g cm^{-3}), with age-specific respiratory deposition (16–20, 21–40, 41–60 years) quantified *via* the multiple-path-particle-dosimetry model for total, regional, and lobar levels. For PM_{10}, the highest deposition fraction (80–95%) occurred in the head region of individuals aged 16–20, while $PM_{2.5}$ showed the highest deposition fraction in the 41–60 age group, particularly in the head (35–90%) and pulmonary (19%) regions. UFPs (<100 nm) are predominantly deposited in the thoracic and pulmonary regions, and the magnitude of UFP deposition in these regions increases with higher welding currents and voltages. SMAW and WAAM processes exhibited the highest particle deposition, with deposition of both PM and UFPs being greatest in the oldest age group. Within the lungs, the lower lobes showed the greatest particle deposition (21%), dominated by UFPs across all age groups. The estimated excess lifetime cancer risk (1.28×10^{-4} to 6.88×10^{-4}) exceeded WHO benchmark thresholds, while hazard quotients for $PM_{2.5}$ (20–88) and PM_{10} (16–81) were significantly above recommended safety limits. These findings underscore the urgent need to regulate occupational exposure and include UFPs in air quality standards.

Received 20th May 2025
Accepted 22nd October 2025

DOI: 10.1039/d5va00142k

rsc.li/esadvances

Environmental significance

Welding processes generate hazardous particulate matter (PM) and ultrafine particles (UFPs) that contribute significantly to workplace air pollution, presenting serious risks to respiratory health and cancer incidence among exposed workers. The impact of these emissions is compounded by evolving industrial techniques and increased automation, which may alter exposure levels and patterns in future occupational environments. A comprehensive understanding of emission characteristics, particle deposition, and exposure pathways is crucial for evaluating the long-term environmental and health implications of welding-related PM and UFPs. This study provides a detailed assessment of fine and UFP emissions across shielded metal arc welding (SMAW), wire arc additive manufacturing (WAAM), and friction stir welding (FSW), identifies current gaps in occupational air quality standards, and emphasises the urgent need to establish robust guidelines for regulating fine and UFP exposures to better safeguard worker health and support sustainable industrial practices.

1. Introduction

Welding fumes, composed of toxic metals such as chromium, nickel, and manganese, pose severe occupational health risks. These fumes, rich in fine particulate matter (PM) and ultrafine particles (UFPs), are a major source of health hazards in industrial environments and are linked to increased risks of premature mortality.[1,2] An estimated 10 million workers worldwide are exposed to these fumes,[3] which have been linked to bronchitis, respiratory irritation, and inflammation.[4–6]

[a]*School of Mechanical Sciences, Indian Institute of Technology (IIT) Goa, Goa College of Engineering Campus, Farmagudi, Goa, 403401, India. E-mail: thaseem@iitgoa.ac.in; Tel: +91-832-2490-859*

[b]*Center of Excellence in Colloids, Particulates and Interfaces, Indian Institute of Technology (IIT) Goa, India*

[c]*Center of Excellence in Sustainable Energy, Indian Institute of Technology (IIT) Goa, India*

[d]*TRIP-Centre, Indian Institute of Technology New Delhi, India*

However, there is no unified occupational exposure limit (OEL) for welding fumes in India or the European Union (EU) for fine and UFPs.[7] Commonly used welding techniques, including shielded metal arc welding (SMAW), wire arc additive manufacturing (WAAM), friction stir welding (FSW), and laser welding, generate substantial volumes of fumes, ranging from 1.7 to 8.3 mg s^{-1} (ref. 8) and are typically rich in both particulate matter (PM) and ultrafine particles (UFPs).[9,10] Their chemical composition varies with the base materials and consumables used, with common constituents including oxides of iron (Fe), manganese (Mn), nickel (Ni), and chromium (Cr). Exposure to these oxides has been linked to serious health risks, including contributions to premature mortality.[1,2,11,12] Metals such as Mn and Ni, due to their high water solubility, are more readily absorbed in the respiratory tract.[13,14] These oxides are primary contributors to adverse cardiopulmonary effects,[9] while respirable PM can increase oxidative stress and trigger inflammatory responses in the respiratory system.[15] Beyond quantifying fume chemical composition concentrations, it is also essential to assess the size distribution of PM and UFPs emitted by different welding techniques, as particle size strongly influences their deposition patterns and associated health impacts. PM concentration is categorised based on aerodynamic diameters of particles commonly encompassing sizes of 10 μm or smaller (PM_{10}), 2.5 μm or smaller ($PM_{2.5}$), 1.0 μm or smaller (PM_1), and less than 0.1 μm, referred to as ultrafine particles (UFPs).[16]

UFPs pose increased toxicological risks due to greater lung deposition, causing significant respiratory and cardiovascular effects.[15] Particles below 30–50 nm can penetrate cells and transport toxins to less-exposed tissues.[17,18] Inhaled PM from welding enters the respiratory tract through the nose or mouth, depositing in the extrathoracic (head (H)), tracheobronchial (TB), and pulmonary (P) regions, creating health issues influenced by particle size and breathing patterns.[19,20] Health risk assessments of PM and UFPs are more accurately determined by their deposition in the respiratory system rather than concentrations of PM and UFPs.[21,22] PM exposure is linked to respiratory and cardiovascular diseases,[23] cerebrovascular impacts,[24] low birth weight,[25] DNA mutations,[26] and kidney disorders, with children and the elderly being most vulnerable.[27,28] While several studies have addressed ambient PM and UFP deposition in outdoor air,[25,29] there is a lack of research on occupational deposition patterns from indoor hazards like welding in both developed and developing countries.

In India, rapid urbanisation and industrial activities, such as welding, contribute to PM levels exceeding regulatory standards, driving increased mortality and morbidity.[30] Welding emissions release PM and UFPs, posing significant occupational health risks to over 10 million workers worldwide, contributing to bronchitis, respiratory irritation, and inflammation.[4,31] PM and UFP concentrations are commonly used to estimate lung deposition in studies, risk assessments, and regulatory evaluations. Deposition depends on factors such as aerosol concentration, respiratory patterns, and particle properties.[32] Notably, the delivered dose is a key metric in toxicological dose–response analysis and is essential for accurate human health risk assessment.[7] Understanding particle deposition in the human respiratory system is crucial for accurately assessing exposure-related health risks. While exposure concentrations are relatively easy to measure, quantifying the delivered dose is more complex. A study underscored the importance of quantifying welding particle deposition to more accurately assess the associated health effects.[33] Dosimetry models, such as the widely used multiple-path particle dosimetry (MPPD) model, provide a practical solution by estimating total, regional, and lobar deposition based on aerosol properties and respiratory parameters.[29,34,35]

Occupational exposure to PM and UFPs from welding poses serious health risks but remains under-researched, particularly in low- and middle-income countries like India. While ambient air quality awareness is growing, the health impacts of different welding techniques and their operational parameters are not well understood. This study examines particle deposition from SMAW, WAAM, and FSW welding processes, considering key factors such as current, voltage, feed rate, and rotational speed. SMAW has been previously investigated in very few studies for PM and UFP emissions; detailed deposition patterns for these particle sizes remain unquantified. Furthermore, emerging industrial welding techniques such as WAAM and FSW have not been sufficiently studied with respect to their emission characteristics or associated health risks. The MPPD model is used to simulate exposure scenarios and assess age-specific deposition of PM and UFPs in the respiratory tracts of males aged 16–20, 21–40, and 41–60 years for different welding techniques. The analysis emphasises the influence of particle size on deposition patterns across the head, tracheobronchial, and alveolar regions. Additionally, the study also assesses potential health risks to workers, using metrics such as excess lifetime cancer risk (ELCR), hazard quotient (HQ), excess risks (ER), and attributable fraction (AF) for all-cause mortality, cardiopulmonary mortality, and lung cancer mortality. This research highlights urgent gaps in occupational air quality regulation for welding, where existing standards focus primarily on respirable PM and largely ignore fine and ultrafine particles that penetrate deeper into the lungs. Our findings underscore the need for updated exposure limits targeting these smaller particles to better protect workers' health.

2. Materials and methodology

2.1 Study area and instrumentation for monitoring

The experimental study was conducted in the central mechanical workshop of an educational institute in India. The workshop features 16 windows for ventilation and a single open entry point serving as the main door. PM and UFP concentrations were measured for various welding techniques, including SMAW, WAAM, and FSW, at two levels: breathing height (1.5 m) and welding height (1.1 m). These measurements were used to analyse PM and UFP behavior as welding fumes disperse from the welding height to the breathing height and other locations within the workshop. UFP concentrations were recorded using a TSI Scanning Mobility Particle Sizer (SMPS) Electrostatic Classifier (Model 3082), while PM concentrations were assessed with the TSI DustTrak DRX Aerosol Monitor (Model 8533) and

a network of low-cost sensors (LCS) equipped with a PMS 5003.[36] The LCS and DustTrak were used to measure $PM_{2.5}$, whereas the SMPS captured the total number concentration (TNC) and particle size distribution within the 15–600 nm range. The present study on the assessment of PM and UFP exposure among workers builds upon our previous work on monitoring emissions from different welding techniques in industrial environments.[37,38]

SMAW was performed using an Aotai ARC200 with adjustable current and constant voltage for a stable arc. The emissions of $PM_{2.5}$ and TNC during SMAW are primarily caused by the electric arc, which heats the base metal and flux coating.[39,40] For SMAW, PM, and UFPs, emissions were measured at two heights using 5 mm mild steel samples under varying current levels: 50 amperes, 75 amperes, 100 amperes, and 125 amperes. Emissions were measured at WH and BH under four conditions, with each test repeated three times. Spatial and temporal variations were recorded in three intervals: pre-welding (7 min), welding (13 min), and post-welding (30–60 min).

WAAM is an advanced metal additive manufacturing technique that builds components by depositing layers of molten metal using a continuously fed filler wire melted by an electric or plasma arc. WAAM is suitable for large, durable parts in the automotive, marine, and aerospace industries. In this study, WAAM was performed using a TAL BRABO TR12-6 robotic arm and a MOGORA INVAMIG 400 MIG welding set on carbon steel to ensure consistent process repeatability. Low and mild-carbon steels are widely used due to their excellent weldability, cost-effectiveness, and availability, although they have lower mechanical and corrosion properties than materials like titanium or superalloys.[41] Alloying elements such as titanium (Ti), copper (Cu), nickel (Ni), and manganese (Mn) are added to enhance strength, toughness, and corrosion resistance.[42] In WAAM, *in situ* interlayer powder alloying can further improve steel properties, making it a key area for research and development in manufacturing ultrahigh-strength steels with tailored mechanical characteristics, and understanding how the emissions are changing with them. For the WAAM process, the evolution of PM and UFP emissions was analysed under two operational conditions: 18 volts and 65 amperes (globular transfer) and 25 volts and 125 amperes (spray transfer). Emissions were evaluated for WAAM with and without the incorporation of CuTi powder, and details of the PM and UFP emissions from these are discussed in ref. 38. Initial measurements were performed with CuTi powder under two conditions: as-received (in its original purchased form) and preheated before addition (more details can be found in ref. 38). Using an electric sieve shaker, the CuTi powder was then classified into three size ranges: <25 μm, 25–45 μm, and 45–95 μm. For each size range, emissions generated during WAAM deposition were assessed under controlled conditions, with a consistent powder quantity used across all experiments. Each experiment involved the deposition of 15 WAAM layers, ensuring a reliable comparison of emission data across the different powder size ranges.[38]

FSW is a solid-state welding process that joins metals without melting them, using a rotating, non-consumable tool to generate frictional heat and bond materials. FSW was conducted using various combinations of feed rate and RPM, including lower feed rate with either lower or higher RPM and higher feed rate with either lower or higher RPM. The deposition of UFPs was carried out using different feed rates of 38 mm min^{-1}, 58 mm min^{-1}, and 95 mm min^{-1}, along with tool rotation speeds of 636, 900, and 1224 RPM, at WH or BH (both are the same).[43] These experiments provided valuable insights into the emission dynamics of PM and UFPs for different welding techniques and parameters. Detailed descriptions of the experimental setup, tested materials, and the industrial relevance of the welding techniques and their respective parameters can be found in ref. 37, 38 and 44.

2.2 Dosimetry model description

The deposition fraction of inhaled PM particles in the human respiratory tract was assessed using the MPPD, Version 3.04 model developed by the Hamner Institutes for Health Sciences, USA. This extensively validated model is widely used in education, research, and industry, making it a reliable tool for airway particle dosimetry.[34,45,46] Its theoretical foundation and applications have been reviewed in several studies,[47,48] and can be accessed *via* the American Research Association (ARA) website. The MPPD model simulates particle deposition across species for particles ranging from 0.001 μm to 100 μm, offering options like Yeh–Schum, stochastic, and age-specific frameworks. This study used the age-specific 5-lobe model for its realistic representation of human airway morphology, capturing structural and respiratory differences between children and adults.[49]

The model incorporates impaction, sedimentation, and diffusion mechanisms to estimate particle deposition in specific respiratory regions—extrathoracic (head), TB, and P.[19] The deposition fraction (DF) in the model refers to the proportion of particles of a specific size that settle in a particular respiratory region (head, TB, or P) relative to the total number entering the airways.[50] Input parameters include particle properties (density and size distribution), exposure conditions, and respiratory features such as breathing frequency (BF), tidal volume (TV), functional residual capacity (FRC), and upper respiratory tract (URT) volume. Also, it was assumed that all particles entered the respiratory system *via* the nose with an upright body orientation. Exposure to PM is categorised into constant and variable scenarios. This study uses average PM and UFP concentrations from different welding conditions under constant exposure. The input parameter values other than PM and UFP concentration were taken from different studies,[51,52] as shown in Table 2. Welding activities are typically performed by individuals across a wide age range, from 16 to 60 years.[32,53] For this study, three distinct age groups were selected: 16–20 years (teenage), 21–40 years, and 41–60 years. The MPPD model results, particularly the deposition fraction (DF), were utilised to estimate particle deposition (in μg or number of particles) using the equation provided in ref. 45.

$$\text{Deposition} = \text{DF} \times C \times T \times V_{\text{E}} \quad (1)$$

Table 1 Defined input parameters and their assigned values for the MPPD model

	Values or options	
	Teens	Adults
Parameters for input	Males	Males
Species	Human	
Model	Age-specific 5 lobe	
Particle properties	Density: 2 g cm^{-3} & 7 g cm^{-3}, aspect ratio: 1, count median diameter: 0.05 μm, GSD: 1, infallibility adjustment: $PM_{2.5}$/PM_{10}/UFPs	
Exposure scenario	Acceleration due to gravity: 9.81 m s^{-2}; body orientation: upright, inspiratory fraction = 0.5; breathing scenario = nasal	
FRC (mL or L)	$0.125 \times 10^{-3} \times h$ height (cm)[3,29]	36 × height (cm) + 3.1 × age (years) − 3183 (ref. 29)
Clearance setting	Number of hours per day = 6; number of days per week = 5; number of weeks = 1/45/2340; max. post-exposure days = 0, tracheal mucous velocity = 5.5 mm min^{-1}; fast human clearance rate = 0.02/day, medium human clearance rate = 0.001/day; slow human clearance rate = 0.0001/day; lymph node human clearance rate = 0.00002/day	

Table 2 Breathing parameters used in the model across different age groups, including tidal volume (TV), upper respiratory tract volume (URTV), V_E (inhalation rate) and breathing frequency (BF)

Age group	FRC (ml)	URTV (ml)	BF (min^{-1})[19]	TV (ml)	V_E (l min^{-1})
16–20 years	2228.9	25	32	416 (ref. 29)	9.06
21–40 years	2832.0	50	20	616 (ref. 58)	11.8
41–60 years	2858.0	50	20	616 (ref. 58)	13.5

In eqn (1), DF represents the deposition fraction of particles, C is the average particle concentration measured during each welding technique and their respective parameters (in μg m^{-3} or particles per cm^3), T is the duration of welding exposure (in minutes), and V_E is the per-minute ventilation rate or inhalation rate (in L min^{-1}), which is calculated using easily measurable variables, as outlined in ref. 54.

$$V_E = e^{-8.57}\mathrm{HR}^{1.72} f_B{}^{0.611}\mathrm{age}^{0.298}\mathrm{sex}^{-0.206}\mathrm{FVC}^{0.614} \quad (2)$$

In this equation, heart rate (HR) is in beats per minute (bpm),[55] breathing frequency (f_B) in breaths per minute,[19] and forced vital capacity (FVC) in liters (mL);[29] age is given in years, and sex is coded as 1 for males. FRC (functional residual capacity) is the volume of air remaining in the lungs after a normal, passive exhalation. Table 1 provides an overview of the input parameters and their assigned values used in the MPPD model to estimate the deposition fraction. Functional residual capacity (FRC) was calculated using a height-based formula for teenagers (16–20 years) and an age-height-based equation for adults (21–60 years), as indicated in Table 1. Table 2 details the parameter values applied in the model across different age groups, including FRC, tidal volume, upper respiratory tract volume, and breathing frequency. Upper respiratory tract volume refers to the total volume of air contained within the upper portions of the respiratory system, including the nasal cavity, pharynx, and larynx.

To investigate how particle size and mass distribution affect deposition fractions, the MPPD model was first applied under the assumption of deposition-only, with no clearance mechanisms included. Regional and lobar deposition fractions were calculated for UFPs, $PM_{2.5}$, and PM_{10} across different age groups. These deposition fraction values formed the basis for estimating the deposition dose of each particle type using the formula in eqn (1), allowing for direct comparison across various age groups. To reflect the range of welding fume properties, deposition calculations were performed with particle densities of 2 g cm^{-3} and 7 g cm^{-3}, spanning from the effective densities of particulates produced by different welding techniques (2 g cm^{-3})[56] to the bulk density of iron (Fe), the primary component of most welding fumes (7 g cm^{-3}).[11] For a robust range-bound analysis, deposition doses for UFPs, $PM_{2.5}$, and PM_{10} were computed for each age group by systematically incorporating the average, minimum, and maximum particle concentrations measured during welding, under both density conditions.

A simulation was conducted using the MPPD model to evaluate welding fume particle retention, encompassing both deposition and clearance. The assessment began with a one-week exposure scenario, designed to reflect typical occupational conditions of six working days with eight hours of full exposure each day.[57] The model incorporated concentrations of $PM_{2.5}$, PM_{10}, and UFPs measured from different welding techniques, analysing each fraction at its average, minimum, and maximum observed levels. To account for variations in fume composition, simulations were performed using particle densities of 2 g cm^{-3} and 7 g cm^{-3}. All input details for these clearance and deposition calculations are provided in Table 1 (clearance settings). To understand the cumulative impact of long-term exposure, the same model parameters were applied in an extended simulation covering a 45 years timespan (equivalent to 2340 working weeks under the same occupational conditions), providing insight into particle retention and clearance dynamics over a typical working lifetime.

2.3 Health risk assessment (HRA)

Exposure to ambient air pollution has been linked to a wide range of health effects, from minor, short-term respiratory issues to more severe conditions such as reduced lung function, activity limitations, and overall diminished performance.[59] This section outlines the framework for assessing pollution-related health risks, beginning with pollutant sources and emissions. The process then moves through environmental concentrations, human exposure levels, and internal doses before ultimately evaluating health impacts.[60,61] Two key methods used to assess health risks associated with PM_{10} and $PM_{2.5}$ exposure are Excess Lifetime Cancer Risk (ELCR) and the Environmental Burden of Disease (EBD) attributable to air pollution.[62] The approach adopted here integrates methodologies from ref. 63 and 64. According to Kim *et al.* (2018),[63] contaminant health risk assessments are categorised into carcinogenic and non-carcinogenic evaluations. The carcinogenic risk is assessed using ELCR for fine particulate matter, as detailed in the following section.

2.3.1 Excess lifetime cancer risk (ELCR). The ELCR is calculated by multiplying the slope factor (SF) by the lifetime average daily dose (LADD). This metric estimates the probability of an individual developing cancer due to long-term exposure to contaminants. The reference value for ELCR is 3.14×10^{-6}, which corresponds to one additional cancer case per one million exposed individuals.[63] The formula for ELCR is expressed in eqn (3):

$$\mathrm{ELCR} = \mathrm{SF} \times \mathrm{LADD} \tag{3}$$

where SF represents the contaminant-specific slope factor ($\mu g\ kg^{-1}\ day^{-1})^{-1}$ and LADD denotes the lifetime average daily dose ($\mu g\ kg^{-1}\ day^{-1}$). This risk assessment tool is crucial in evaluating potential carcinogenic hazards associated with environmental pollutant exposure.

(a) Slope factor (SF). The United States Environmental Protection Agency (USEPA)[65] supplies the SF data for each contaminant, which can be calculated using the following formula:

$$\mathrm{SF} = \frac{\mathrm{UR}}{\mathrm{BW} \times \mathrm{IR}} \tag{4}$$

where UR = unit risk of $PM_{2.5}$ ($\mu g\ m^{-3}$), BW is body weight (kg), IR = inhalation rate ($m^3\ day^{-1}$) (IR refers to the total volume of air a person breathes in over the course of a day, measured in cubic meters per day), and SF = slope factor ($\mu g\ kg^{-1}\ day^{-1})^{-1}$.

(b) Lifetime average daily dose (LADD). The LADD represents the cumulative exposure of occupants to contaminants over their lifespan, and its calculation is as follows:

$$\mathrm{LADD} = \frac{\mathrm{CA} \times \mathrm{IR} \times \mathrm{EF} \times \mathrm{ED}}{\mathrm{BW} \times \mathrm{AT}} \tag{5}$$

where CA is the contaminant concentration ($\mu g\ m^{-3}$), IR is the inhalation rate ($m^3\ day^{-1}$), EF is the exposure frequency (days $year^{-1}$), ED is the exposure duration (years), BW is the body weight (kg), and AT is the averaging time (days) (Table 3). For the calculation of LADD, the average $PM_{2.5}$ concentrations from different welding techniques and their respective parameters were used as input. The LADD approach does not account for particle deposition in specific regions of the respiratory system; instead, risk is derived directly from exposure concentrations.

The risk assessment assumed an 8 hours exposure duration to represent a standard full work shift. This duration is based on the widely accepted occupational exposure limit framework, which uses an 8 hours time-weighted average as a benchmark exposure period for industrial environments.[66] This approach corresponds with regulatory guidelines and common industrial hygiene practices for welding, where an 8 hours daily exposure is typical for workers. For modelling purposes, it was assumed that welding activity occurred continuously throughout this 8 hours period to provide a conservative estimate of exposure.[67] The concentrations of PM and UFPs used in the risk assessment are derived from actual measurements performed in our prior studies. These measurements were process-specific and condition-specific, capturing PM and UFP emission rates from various welding techniques under defined operating parameters.[37,38] For the prediction of LADD and ELCR, we assumed a constant average exposure based on these measurements. Although spatial and temporal variations were monitored during pre-welding (7 min), welding (13 min), and post-welding (30–60 min) intervals, only the concentrations recorded during active welding were considered for exposure estimation. This average concentration was then used to predict the exposure for an 8 hours work shift, providing a representative basis for evaluating occupational health risks.

2.3.2 $PM_{2.5}$ exposure index. The $PM_{2.5}$ exposure index was determined for each activity using a 1 hour activity record, offering a detailed evaluation of how PM emissions from various welding techniques impact occupational workers in industrial settings.

$$E_i = \sum \frac{W_{P_{P_i}} \times t_k}{W_g \times t_a} \tag{6}$$

where E_i is the exposure index, $W_{P_{P_i}}$ is the average $PM_{2.5}$ concentration ($\mu g\ m^{-3}$) for the specific operating parameter of a welding technique, t_k is the time spent by workers in that specific environment, W_g is the $PM_{2.5}$ guideline concentration (WHO) (15 $\mu g\ m^{-3}$),[71] and t_a is aggregate time (8 hours) (Table 3).

2.3.3 Intake concentration. In addition to estimating SF, LADD, and ELCR, the intake concentration and hazard quotient were also calculated to assess exposure levels. The average time (in hours) workers spent in the kitchen was determined from their daily activity logs. As per the updated USEPA guidelines,[72] the inhalation rate and body weight are excluded when calculating the intake dose of airborne contaminants. The potential intake concentration is determined using the following equation.

$$\mathrm{IC} = \frac{\mathrm{CA} \times \mathrm{ET} \times \mathrm{EF} \times \mathrm{ED}}{\mathrm{AT}} \tag{7}$$

The intake concentration (IC) is determined using several key parameters, including the contaminant concentration (CA) in $\mu g\ m^{-3}$, exposure frequency (EF) in days $year^{-1}$, the exposure

Table 3 Definition, source of information, and typical values

Parameters	Definition and units	Values	References
BW	Body weight (kg)	16–20 years: 50 20–60 years: 70	USEPA[68] USEPA[68]
IR	Inhalation rate (m^3 day^{-1}) or V_e	16–20 years: 9.06 21–40 years: 11.84 41–60 years: 13.59	Greenwald (2019)[54]
EF	Exposure-frequency (days $year^{-1}$)	270 days	Present study
UR	Unit-risk ($PM_{2.5}$) (μg m^{-3})	0.008	63 and 69
ED	Exposure-duration (years)	15	70
SF	Slope-factor (μg kg^{-1} day^{-1})		USEPA[65]
AT	Averaging-time (days)	Non-carcinogens AT = ED × 365 days $year^{-1}$ Carcinogens AT = 70 year × 365 days $year^{-1}$	64 and 69
ELCR	Excess lifetime cancer risk	Calculated values	63
LADD	Lifetime-average-daily-dose (μg kg^{-1} day^{-1})	Calculated values	69
ET	Exposure-time (hours day^{-1})	8	70
IC	Intake-concentration (μg m^{-3})	Calculated values	70
Rfc	Reference-concentration (μg m^{-3})	$PM_{2.5}$: 40, PM_{10}: 68	Background concentration during experiments
HQ	Hazard quotient	Calculated values	70
β	Coefficient-of-risk-function	0.155 (95% CI: 0.056–0.25) for cardiopulmonary-mortality, 0.232 (95% CI: 0.085–0.378) for lung-cancer-mortality, and 0.0008 (95% CI: 0.0006–0.001) for all-cause-mortality	64 and 69
X_0	Baseline concentration (μg m^{-3})	$PM_{2.5}$: 40, PM_{10}: 68	Background concentration during experiments

time (ET) in hours day^{-1}, the exposure duration (ED) in years, and the average time (AT) in days (Table 3).

2.3.4 Hazard quotient (HQ). The hazard quotient (HQ) is used to assess the potential non-carcinogenic health effects associated with $PM_{2.5}$ exposure. It is calculated by comparing the intake concentration (IC) in μg m^{-3} to the reference concentration (RFC) in μg m^{-3}, following the methodology outlined in ref. 65 and 70. A hazard quotient value greater than 1 indicates a potential risk of adverse health effects, while a value below 1 suggests minimal risk.

$$HQ = \frac{IC}{RFC} \quad (8)$$

2.3.5 Relative risk (RR), excess risk (ER), and attributable fraction (AF). The Environmental Burden of Disease (EBD) framework involves the estimation of key epidemiological metrics, such as relative risk (RR), excess risk (ER), and attributable fraction (AF). The RR for all-cause mortality due to short-term exposure to PM_{10} was determined using the equation proposed in ref. 73. RR represents the likelihood of adverse health effects, such as all-cause mortality or lung cancer mortality, in a population exposed to elevated air pollution levels compared to a background level with minimal anthropogenic pollution (68 μg m^{-3} for PM_{10}). Further details on RR, ER, and AF can be found in Section S1 of the SI.

3. Results and discussion

3.1 Summary of variation in PM and UFP concentrations during different welding processes

Tables 4, S1 and S2 provide a summary of the average UFP, $PM_{2.5}$, and PM_{10} concentrations for SMAW, WAAM, FSW, and their respective parameters. The UFP concentration is expressed as the TNC within the particle size range of 15 nm to 589.2 nm for each welding technique. The emissions of $PM_{2.5}$ and TNC during SMAW mainly originate from the electric arc, which intensely heats the base metal and flux coating.[39,40] The flux coating, composed of metallic oxides, silicates, and organic binders, undergoes combustion and vaporisation at these high temperatures.[4] This process releases gases, vapours, and particulate matter, which significantly contribute to the measured emissions. During SMAW, $PM_{2.5}$ and PM_{10} concentrations were lowest at 50 amperes and highest at 125 amperes, with UFP TNC also peaking at 125 amperes and dropping to the minimum at 50 amperes. During WAAM, both $PM_{2.5}$ and PM_{10} concentrations peaked at lower current and voltage settings, while UFP TNC was higher under lower operating conditions than higher currents and voltages. The results from various test conditions for FSW reveal that lower feed rates combined with lower or higher RPMs (38 mm min^{-1} and 636 rpm or 1224 rpm) tend to increase UFP emissions. Conversely, at higher feed rates combined with lower or higher RPMs (95 mm min^{-1} and 636 rpm or 1224 rpm), UFP emissions are also high. Interestingly, when the feed rate is maintained at 58 mm min^{-1}, UFP emissions remain low, regardless of whether the RPM is high or low. The variation in UFP emissions is mainly driven by particles smaller than 100 nm, while concentrations of particles larger than 100 nm decrease sharply. As a result, $PM_{2.5}$ and PM_{10} levels remain close to ambient values across different FSW operating conditions. Therefore, deposition analysis for FSW was focused on UFPs in the 10–600 nm range.[37]

Table 4 Variation of PM and UFP concentrations during different welding techniques with their respective parameters (more details on the PM and TNC values for different welding techniques are provided in Tables S1 and S2 in the SI) (A: amperes)

Welding techniques	Welding techniques and parameters	TNC (#/cm^3)	$PM_{2.5}$	PM_{10}
SMAW	50 A SMAW	1.30×10^6	650	900
	75 A SMAW	1.49×10^6	1210	1890
	100 A SMAW	1.37×10^6	2380	3840
	125 A SMAW	2.36×10^6	2780	4350
WAAM	18 volts, 65 AWAAM	2.7×10^6	1300	2200
	20 volts, 125 A WAAM	1.44×10^6	910	1850
		TNC (#/cm^3)		
FSW	38 mm min^{-1} to 1224 RPM	1.35×10^7		
	38 mm min^{-1} to 900 RPM	7.16×10^6		
	38 mm min^{-1} to 636 RPM	5.62×10^6		
	95 mm min^{-1} to 1224 RPM	1.15×10^7		
	95 mm min^{-1} to 900 RPM	2.31×10^6		
	95 mm min^{-1} to 636 RPM	5.38×10^6		
	58 mm min^{-1} to 1224 RPM	5.50×10^6		
	58 mm min^{-1} to 636 RPM	2.31×10^6		

3.2 Particulate matter deposition estimates

3.2.1 Total particulate matter deposition fraction in human airways. The DF of PM_{10}, $PM_{2.5}$, and UFPs across various age groups for different particle density values is summarised in Fig. 1, calculated using parameters such as FRC, URT, BF, and TV as explained in Tables 1 and 2. Regarding total DF ($DF_{total} = DF_{head} + DF_{TB} + DF_P$), PM_{10} demonstrated the highest total DF in the human respiratory tract, ranging from 96% to 100% (Fig. 1f), followed by $PM_{2.5}$, which ranged between 55% and 98% (Fig. 1e) across different age groups and different densities. For PM_{10}, most particles were deposited in the head region compared to the tracheobronchial and pulmonary regions, with deposition increasing as density rose to 7 g cm^{-3} (Fig. 1f). This is due to greater inertia and faster settling of high-density particles, leading to enhanced impaction and sedimentation in the nasal passages and larynx (head region). For $PM_{2.5}$, deposition was also highest in the head region.[74,75] At 2 g cm^{-3}, some increase was observed in the pulmonary region, but at 7 g cm^{-3}, deposition shifted predominantly to the head with reduced pulmonary deposition (Fig. 1e). Lower-density $PM_{2.5}$ particles, having smaller aerodynamic diameters, remain suspended longer and diffuse deeper into the lungs, whereas higher-density particles settle more quickly, limiting deep lung penetration.[74,75]

For UFPs, the total DF varied significantly depending on particle size and density: 2 g cm^{-3} particles between 10 and 23 nm showed deposition fractions of 83% to 65%, particles from 23 to 100 nm ranged from 63% to 30%, those between 100 nm and 300 nm exhibited deposition fractions from 29% to 17%, and those between 300 nm and 600 nm exhibited deposition fractions from 17% to 22% (Fig. 1d). 7 g cm^{-3} particles between 10 and 23 nm showed deposition fractions of 64% to 80%, particles from 23 to 100 nm ranged from 63% to 28%, those between 100 nm and 300 nm exhibited deposition fractions from 28% to 25%, and those between 300 nm and 600 nm exhibited deposition fractions from 25% to 51% (Fig. 1e). The higher deposition fraction of UFPs in the pulmonary region at 2 g cm^{-3} compared to 7 g cm^{-3} is due to lower-density particles having smaller aerodynamic diameters, which enhances diffusion and allows deeper lung penetration.[74,75] In contrast, higher-density particles settle faster, reducing their deposition in the deep lungs. Conversely, deposition in the head region is greater at 7 g cm^{-3}, where heavier particles settle more rapidly. Overall, PM_{10} showed higher total deposition percentages than $PM_{2.5}$ and UFPs (Fig. 1f). This density-dependent shift reflects how particle behaviour influences regional lung deposition.

The higher PM_{10} DF in the 16–20 age group may be due to smaller airway dimensions and higher breathing frequency (Table 2), which enhance particle impaction in the upper airways. In contrast, lower $PM_{2.5}$ and UFP deposition in this group likely results from their greater lung volumes and faster clearance, reducing retention. Interestingly, for UFPs, the 16–20 age group had the lowest deposition fractions, while higher fractions were observed in the 21–40 and 41–60 age groups. Overall, males in the 41–60 and 21–40 age groups were found to have greater exposure across all PM sizes compared to those in the 16–20 age group. The higher deposition fractions for PM and UFP in the 21–40 and 41–60 age groups may be linked to age-related changes in lung morphology and reduced clearance efficiency. Additionally, males in these older groups show greater exposure across PM sizes, possibly due to differences in lung size, higher inhalation rate compared to the younger age group (Table 2), breathing patterns, and occupational or lifestyle factors affecting inhalation exposure.[19,76] However, this ranking could change if the analysis focused on specific particle sizes. Despite variations in the methodologies, equations, and assumptions used in previous studies to estimate PM deposition, no significant differences in total DF have been reported across studies.[76–79]

This study also evaluated the deposited mass (Fig. S1) and mass per unit area (Fig. S2 and S3) for SMAW and WAAM under varying current and voltage conditions. PM_{10} exhibited the peak

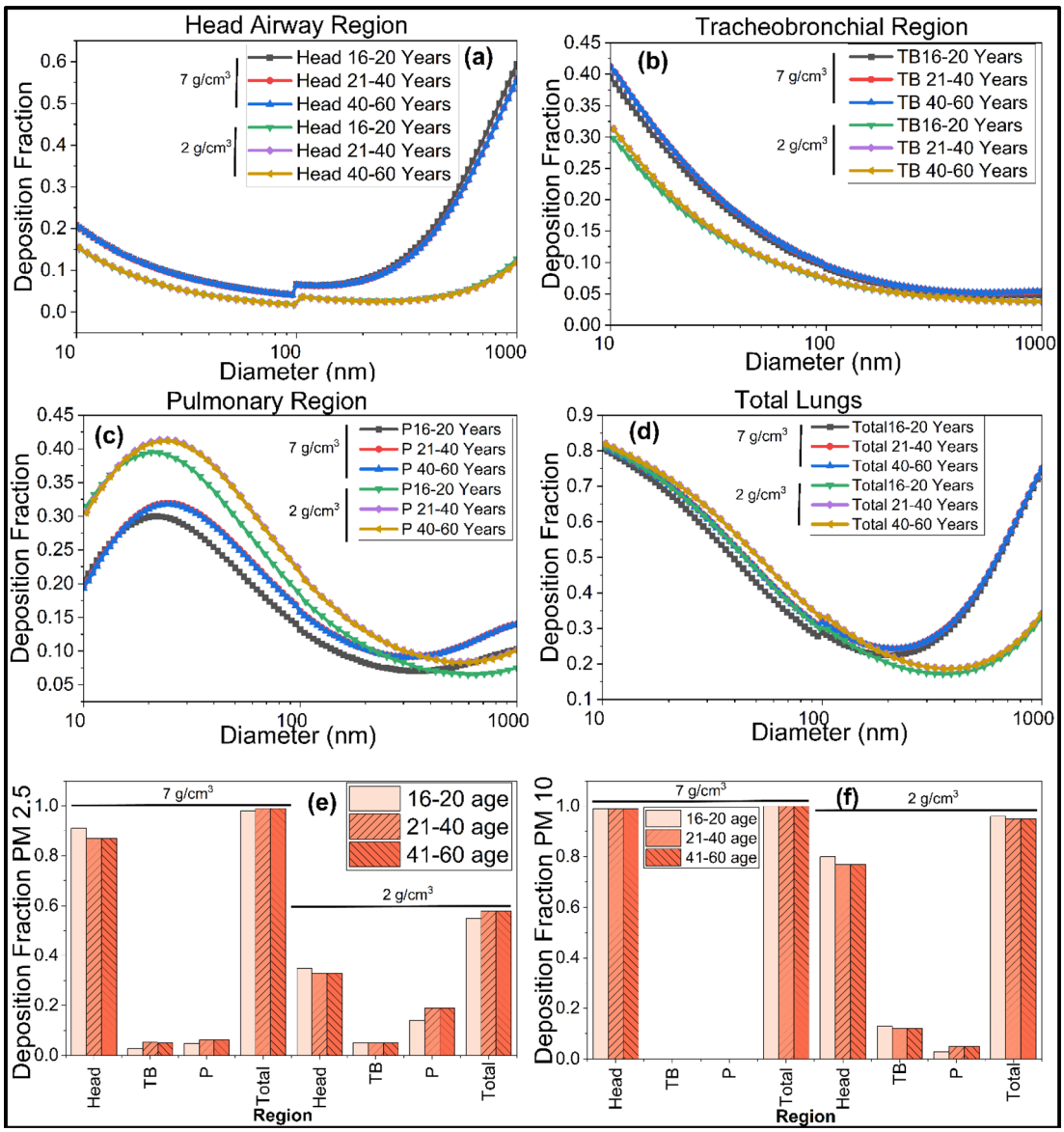

Fig. 1 Influence of age on regional deposition fractions for ultrafine particles (UFPs) and particulate matter (PM) at varying particle densities: (a) deposition in the head region for UFPs (0.01–1 μm), (b) tracheobronchial (TB) region for UFPs (0.01–1 μm), (c) pulmonary (P) region for UFPs (0.01–1 μm), (d) total lung deposition for UFPs (0.01–1 μm), (e) $PM_{2.5}$ across respiratory regions, and (f) PM_{10} across respiratory regions.

value of deposition in the TB region due to its larger particle size compared to $PM_{2.5}$. During SMAW, peak PM_{10} deposition in the TB region occurred across all amperages, with the 16–20 age group recording peak deposition masses of 2.8×10^{-3} μg, 5.9×10^{-3} μg, 0.0121 μg, and 0.0137 μg at 50, 75, 100, and 125 amperes, respectively (Fig. S1). The peak $PM_{2.5}$ deposition, in contrast, showed an increasing trend with age. The 16–20 age group exhibited the peak value of $PM_{2.5}$ deposition, which was lowest across all amperages, ranging from 5.8×10^{-4} μg to 2.4×10^{-3} μg, while the 21–40 and 41–60 age groups recorded average increases of 5% and 6%, respectively, for peak $PM_{2.5}$ deposition in the TB region (Fig. S1). Additional details on SMAW and WAAM peak deposition trends for $PM_{2.5}$ and PM_{10}, along with visualisation of PM deposition in the TB region, are provided in Section 1.1 of the SI.

3.2.2 Regional deposition fraction and deposition of mass for PM and UFPs in human airways. Regarding regional DF, PM sizes and density vary significantly in their deposition across the head, TB, and P. PM_{10} and $PM_{2.5}$ predominantly deposited in the head region for all age groups, with a DF of 88 ± 10% for PM_{10} and 61 ± 20% for $PM_{2.5}$ across different densities, aligning with findings from other studies.[19,29] In contrast, UFPs (0.01 μm to 0.1 μm) showed minimal deposition in the head region (6 ± 1.5%) but were heavily deposited in the P region (30 ± 4.5%). PM_{10} and $PM_{2.5}$ had the least deposition in the pulmonary region at 2 ± 1.5% and 11 ± 6%, respectively. Deposition in the TB region was comparatively lower, with UFPs (0.01 to 1 μm) (12 ± 2%) leading, followed by PM_{10} (6 ± 5%) and $PM_{2.5}$ (5 ± 1%). The standard deviations reflect the variability in deposition fractions for PM and UFPs across different particle densities.

The deposition of welding particles in the respiratory tract is governed by particle size, airflow dynamics, and anatomical characteristics. Different mechanisms dominate across size ranges: inertial impaction favors larger particles (*e.g.*, PM_{10}) in the upper airways, where airflow is strongest,[20,49,50] while ultrafine particles (<100 nm) readily penetrate to the peripheral lung due to Brownian diffusion, posing greater health risks.[48] The total deposition fraction (DF) is highest for 10–250 nm particles, decreases to 300 nm, and then rises to 1000 nm as sedimentation and impaction dominate. Particles deposited in the upper airways are more rapidly cleared, whereas those reaching deeper lung regions persist longer. The calculated size-fraction deposition doses for total and regional deposition (head, TB, and P regions) across all age groups and welding parameters are shown in Fig. 2, 3 and S4.

(a) Deposition of PM_{10} and $PM_{2.5}$ across SMAW and WAAM welding techniques under varying operational parameters. PM_{10} and $PM_{2.5}$ deposition from SMAW increased with amperage across all age groups. In the 16–20 age group, PM_{10} deposition rose from 5.1 ± 0.9 mg at 50 amperes to 24 ± 5.4 mg at 125 amperes in the head region, which is accumulating the most. $PM_{2.5}$ deposition followed a similar trend, increasing from 2.5 ± 1.3 mg at 50 amperes to 11 ± 5.6 mg at 125 amperes in the head region, which is accumulating the most. For the 21–60 age group, PM_{10} deposition (mg) was increased by 380% in the head, TB, and P as the current rating during SMAW was increased from 50 amperes to 125 amperes, while $PM_{2.5}$ deposition is increased by 308% in the head, TB, and P as the current rating during SMAW was increased from 50 amperes to 125 amperes (Fig. 2). These percentage values represent the relative increase in deposition (mg) of PM_{10} and $PM_{2.5}$ between the 50 amperes and 125 amperes levels for each age group, and for different regions of the respiratory system (head, TB, and P). The average and standard deviation (SD) presented in Fig. 2 represent the mean deposition doses for $PM_{2.5}$ and PM_{10}, calculated according to eqn (1).

For each scenario, PM concentrations at their average, minimum, and maximum levels were combined with DF corresponding to two different particle densities, generating six deposition dose values. These values were then averaged, and the SD was calculated to produce the results shown in the figure. The compositional analysis of fumes generated during SMAW identified metal oxides such as iron (Fe), aluminum (Al), zinc (Zn), chromium (Cr), manganese (Mn), nickel (Ni), copper (Cu), and lead (Pb).[80] The study also found that manganese and zinc were more prevalent in the fine and ultrafine particle ranges, with their concentrations increasing alongside rising welding current, likely due to enhanced electrode melting.[80] The increase in PM_{10} and $PM_{2.5}$ deposition with rising current from 50 to 125 amperes during SMAW is due to the higher heat input

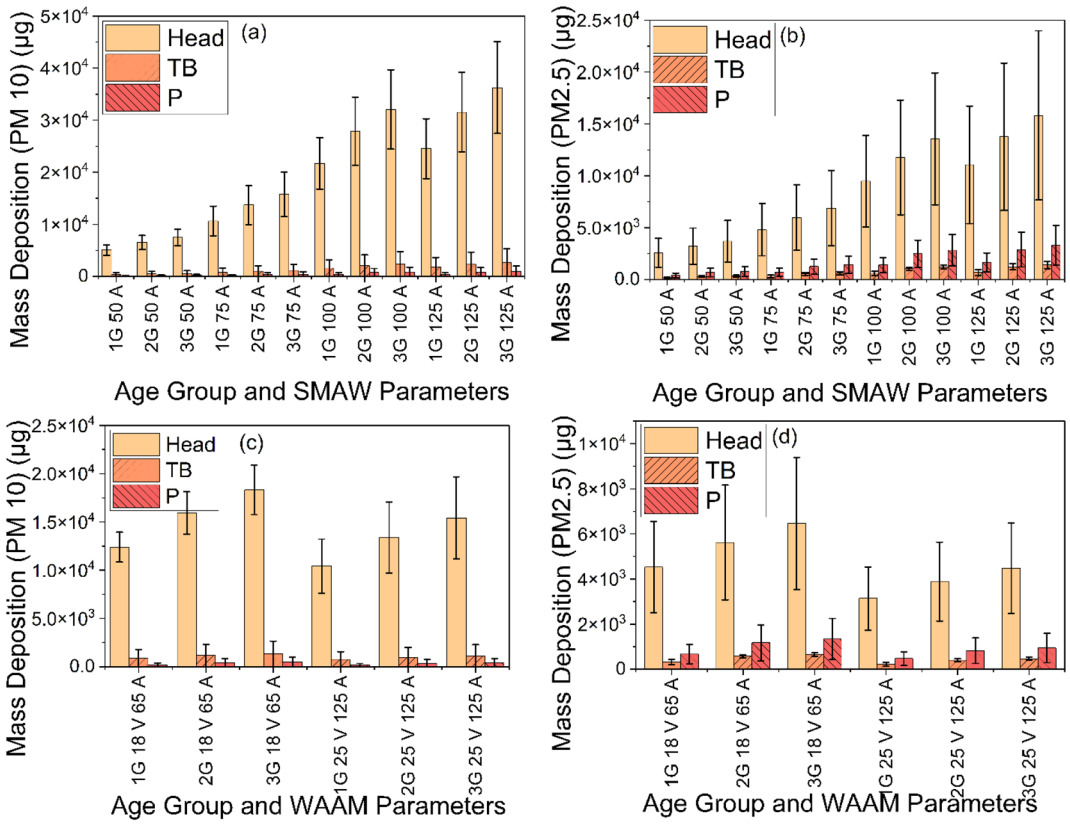

Fig. 2 Deposited mass of PM in the head, tracheobronchial (TB), and pulmonary (P) regions across age groups (1G = 16–20 years, 2G = 21–40 years, 3G = 41–60 years) for different welding techniques and parameters: (a) PM_{10} during shielded metal arc welding (SMAW) at 50 A, 75 A, 100 A, and 125 A, (b) $PM_{2.5}$ during SMAW at 50 A, 75 A, 100 A, and 125 A, (c) PM_{10} during wire additive arc manufacturing (WAAM) at 18 V and 65 A and 25 V and 125 A, and (d) $PM_{2.5}$ during WAAM at 18 V and 65 A and 25 V and 125 A. (A = amperes, V= volts).

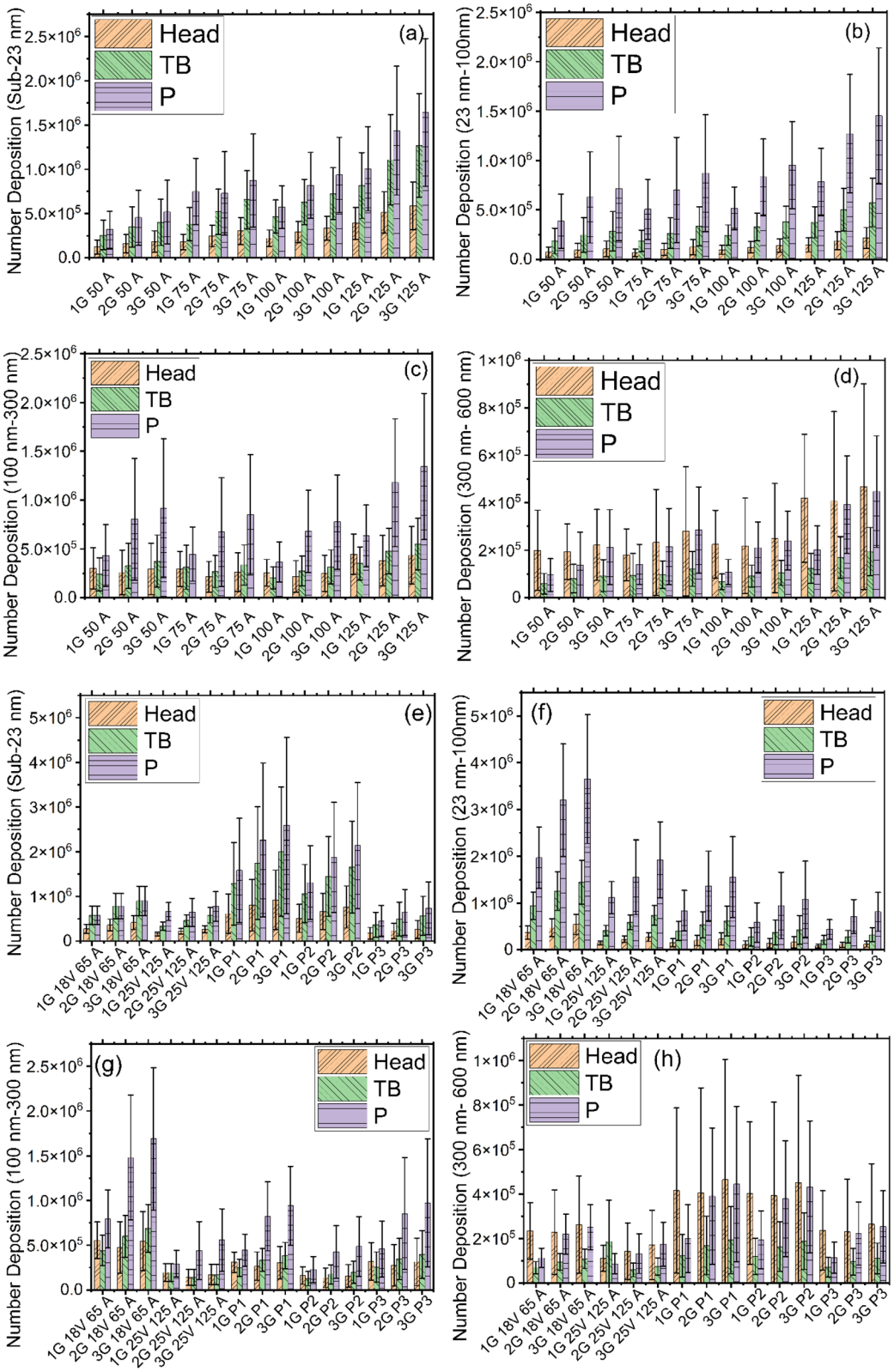

Fig. 3 Deposited number of UFPs for four size ranges (1: sub 23 nm, 2: 23–100 nm, 3: 100–300 nm, 4: 300–600 nm) in the head, tracheobronchial (TB), and pulmonary (P) regions across age groups (1G = 16–20 years, 2G = 21–40 years, 3G = 41–60 years) for shielded metal arc welding (SMAW) (50 A, 75 A, 100 A, and 125 A) and wire additive arc manufacturing (WAAM) (18 V 65 A, 25 V 125 A), WAAM with powders (P1: 95–45 μm, P2: 45–25 μm, and P3: less than 25 μm). ((a) Deposition dose for the sub 23 nm UFP range from SMAW. (b) Deposition dose for the 23–100 nm UFP range from SMAW. (c) Deposition dose for the 100–300 nm UFP range from SMAW. (d) Deposition dose for the S300–600 nm UFP range from SMAW. (e) Deposition dose for the sub 23 nm UFP range from WAAM. (f) Deposition dose for the 23–100 nm UFP range from WAAM. (g) Deposition dose for the 100–300 nm UFP range from WAAM. (h) Deposition dose for the 300–600 nm UFP range from WAAM).

from the electric arc, which boosts combustion and vaporisation of the flux and base metal. This intensifies particulate emissions. Electrode consumption also rises with current, from five electrodes at 50 amperes to twelve at 125 amperes (same interval of welding), reflecting faster melting and material transfer.[37] Higher current enhances arc stability and electrode wear, leading to increased particle generation and thus greater PM emissions. The increase in PM_{10} and $PM_{2.5}$ deposition with age is due to higher inhalation rates in older adults compared to younger individuals. A greater inhalation rate means more air, and consequently more particles, enter the respiratory system, resulting in increased particle deposition in the lungs of older people. Ageing also causes small airways to close at higher lung volumes, trapping more particles in the peripheral lung during exhalation manoeuvres, increasing peripheral deposition.

PM_{10} and $PM_{2.5}$ deposition (mg) in WAAM varied with voltage and amperage. In the 16–20 age group, PM_{10} deposition was 12 ± 1.5 mg at 18 V 65 A (low current and voltage) and 10 ± 1.8 mg at 25 V 125 A (higher current and voltage), while $PM_{2.5}$ deposition was 4.5 ± 2.0 mg and 3.1 ± 1.3 mg, respectively. Deposition increased in older age groups, with PM_{10} deposition (mg) rising from 25 V 125 A to 18 V 65 A by 18% (head), 18% (TB), and 18% (P) in the 21–60 group. $PM_{2.5}$ deposition (mg) rose from 25 V 125 A to 18 V 65 A by 44% (head), 42% (TB), and 42% (P) in the 21–60 group. These percentage values represent the relative increase in deposition (mg) of PM_{10} and $PM_{2.5}$ between 25 V 125 A and 18 V 65 A levels for each age group, and for different regions of the respiratory system (head, TB, and P). In short-circuit or globular transfer mode (low current and voltage), larger, unstable molten droplets are transferred across the arc, causing spatter and oxidation. This unstable transfer leads to droplet detachment and splashing, resulting in higher $PM_{2.5}$ and PM_{10} deposition. In spray transfer (higher current and voltage), smaller droplets are transferred smoothly across the arc, typically at higher currents and voltages, leading to lower $PM_{2.5}$ and PM_{10} deposition. In WAAM, higher current and voltage settings were associated with increased concentrations of iron (Fe) oxides, while manganese (Mn) concentrations were elevated at lower current and voltage levels, contributing more substantially to fine and ultrafine particle emissions under these conditions.[9]

(b) Deposition of UFPs across SMAW, WAAM, and FSW welding techniques under varying operational parameters. UFP analysis categorised particles (15–600 nm) into four size groups, with inhalation doses calculated for different welding techniques. Results show the highest UFP deposition in the P region, unlike PM_{10}, which primarily deposits in the head. $PM_{2.5}$ also deposits more in the P region than the head, but remains lower than the UFP deposition. Fig. 3 shows UFP deposition across respiratory regions for different age groups during SMAW and WAAM, while Fig. S4 presents results for FSW. In SMAW, particles <100 nm deposited more efficiently in the TB and P regions for the 16–20 age group, whereas particles >100 nm dominated in the head region. For the 21–60 age group, particles <100 nm consistently showed higher deposition across all regions. From 50 to 125 A, deposition of <100 nm UFPs increased by ~174–175% in the head, 169% in TB, and 150–154% in P, while >100 nm UFPs increased by ~80–90% across regions. These percentages represent the relative change in particle number deposition from 50 to 125 A, calculated for <100 nm (sub-23 nm, 23–100 nm) and >100 nm (100–300 nm, 300–600 nm) particles across respiratory regions (head, TB, P) and age groups. The average and standard deviation (SD) presented in Fig. 3 and S4 represent the mean deposition doses for UFPs across four size ranges (sub-23 nm, 23–100 nm, 100–300 nm, and 300–600 nm), calculated using eqn (1). UFP concentrations from SMAW, WAAM, and FSW at different parameters were analysed using average, minimum, and maximum values for each size range. Combining these with deposition fractions for two particle densities yielded six dose values, which were averaged with SD (Fig. 3). Results show that smaller particles, especially those <100 nm, deposit predominantly in the P region because of their very small size, which enables them to reach deep lung areas through Brownian diffusion, allowing them to penetrate deeply and deposit in alveoli. As particle size increases, inertial impaction and gravitational sedimentation become dominant, causing larger particles to deposit earlier in the respiratory tract, especially in the head region (nasal passages and upper airways).

Deposition increases with welding current and age, highlighting higher risks for older welders and at higher amperages. This underscores the need for protective equipment and effective ventilation to reduce exposure.

During WAAM, particles <100 nm show higher deposition across all respiratory regions compared to larger UFPs. In the 16–20 age group, deposition of <100 nm particles increased by 110% (head), 103% (TB), and 50% (P) when the current decreased from 125 A 25 V to 65 A 18 V, while >100 nm particles showed greater increases in the head regions. Similar trends occurred in the 21–60 age group, highlighting the influence of welding parameters on deposition. These percentages show relative changes in particle number deposition with current variation (125 A 25 V to 65 A 18 V), calculated for <100 nm and >100 nm particles across respiratory regions and age groups. The inclusion of Cu–Ti powder during WAAM increases ultrafine particle deposition in the respiratory regions due to vaporisation and oxidation of the powder at high arc temperatures, generating metallic oxides. The added powder also provides extra metal surface area that promotes vaporisation and particle formation. Interaction with the arc plasma creates thermal gradients and microexplosions, amplifying particle release and increasing UFP emissions. Using powders of different size ranges for WAAM (95–45 μm, 45–25 μm, and <25 μm), deposition for particles <100 nm is higher in all age groups than for larger UFPs greater than 100 nm. The number deposition was higher at 18 volts 65 amperes and finer powder sizes (45–25 μm), indicating a higher number of particles deposited in the head, TB, and P than other parameters. Older age groups (21–40 and 41–60) are more vulnerable, showing greater deposition than younger individuals (16–20).

During FSW, UFP deposition was notably higher for particles smaller than 100 nm, with the most significant increases observed in the TB and P regions, as shown in Fig. S4. Fig. S4 displays the number deposition of UFPs across four size

ranges—sub-23 nm, 23–100 nm, 100–300 nm, and 300–600 nm—in the head, TB, and P regions. The results indicate that, in terms of the number of deposited particles in the head, TB, and P regions, individuals in the older age group (41–60) experience greater exposure compared to those in the younger age group (16–20). At a feed rate of 38 mm min^{-1}, the total number deposition was highest at 1224 RPM, followed by 900 RPM and 636 RPM. At a 95 mm min^{-1} feed rate, the total number deposition was highest at 1224 RPM, followed by 636 RPM and 900 RPM. In general, the number deposition was higher at the lower and higher feed rates (38 and 95 mm min^{-1}) for their respective RPM values, whereas at the intermediate feed rate of 58 mm min^{-1}, deposition was the lowest across different RPMs (Fig. S4).

3.2.3 PM and UFPs' lobar deposition in human airways. Fig. 4 shows the DF across the five lung lobes at different particle densities across different age groups. The right lung has three lobes—right lower (RL), middle (RM), and upper (RU)—while the left lung has two—left lower (LL) and upper (LU)—to accommodate the heart (as noted in ref. 76). $PM_{2.5}$ showed the highest DF in the lower lobes (LL: 9%, RL: 6%), with the lowest in the RM (1%) across all ages at 2 g cm^{-3}. PM_{10} had lower deposition overall but followed a similar pattern, highest in the lower lobes (LL: 2%, RL: 1%) and lowest in RM (0.45%). At higher particle density (7 g cm^{-3}), both $PM_{2.5}$ and PM_{10} deposition in lobes were very low, concentrating mainly in the head region.

UFPs had notably higher DF, with the LL lobe showing the greatest deposition (13%), followed by RL (9%), and the RM lobe the lowest (2.6%), consistent for all age groups. Additionally, UFPs smaller than 100 nm demonstrated a higher deposition fraction compared to those larger than 100 nm, as indicated in Fig. 4b. The lower lobes of the lungs are more exposed to UFPs, $PM_{2.5}$, and PM_{10} because they receive a larger share of airflow, leading to higher particle delivery and deposition. This is enhanced by gravity-driven settling, slower airflow that promotes sedimentation, and airway geometry that directs more air, and thus more particles, toward these regions.[48,77] The left lung lobes receive higher deposition of UFPs, $PM_{2.5}$, and PM_{10} due to their longer, narrower bronchus with sharper branching angles. This geometry channels more particle-laden airflow, increases inertial impaction, slows airflow, and prolongs particle residence time, all of which enhance deposition compared to the right lung.[81–83]

Notably, the deposition patterns of PM and UFPs also varied with age. Individuals aged 16–20 years showed the lowest deposition, while those aged 41–60 years exhibited the highest, as shown in Fig. 4. This variation in PM deposition among the lobes is attributed to differences in path lengths and lobar volumes; the lower lobes, having larger volumes, experienced greater PM deposition, while the smaller volumes of the middle lobes resulted in lower deposition.[22,77,84] Among the particulate matter types, UFPs less than 100 nm consistently showed the highest deposition fractions across all five lobes in the evaluated age groups. The average UFPs less than 100 nm DF for the LU, LL, RU, RM, and RL lobes were 0.076, 0.19, 0.07, 0.04, and 0.138, respectively, for a density of 2 g cm^{-3}. The average UFPs more than 100 nm deposition fractions for the LU, LL, RU, RM, and RL lobes were 0.023, 0.06, 0.02, 0.01, and 0.04, respectively, for a density of 2 g cm^{-3}. The average UFPs less than 100 nm DF for the LU, LL, RU, RM, and RL lobes were 0.076, 0.14, 0.03, 0.04, and 0.14, respectively, for a density of 7 g cm^{-3}. The average UFPs more than 100 nm deposition fractions for the LU, LL, RU, RM, and RL lobes were 0.13, 0.45, 0.02, 0.01, and 0.04, respectively, for a density of 7 g cm^{-3}.

Fig. S5 illustrates the mass deposition of $PM_{2.5}$ and PM_{10} from SMAW and WAAM across different lung lobes under various operating parameters. Across all operating parameters and welding techniques, the left lower lobe (LL) and right lower lobe (RL) generally show higher PM deposition than the upper or middle lobes, as shown in Fig. S5. The right middle lobe (RM) consistently exhibits the lowest PM deposition. As age increases from 1G (16–20 years) to 3G (41–60 years), the mass of PM deposited in all lung lobes tends to increase for both $PM_{2.5}$ and PM_{10}, indicating that older individuals are at greater risk of particulate deposition during welding fume exposure. Higher

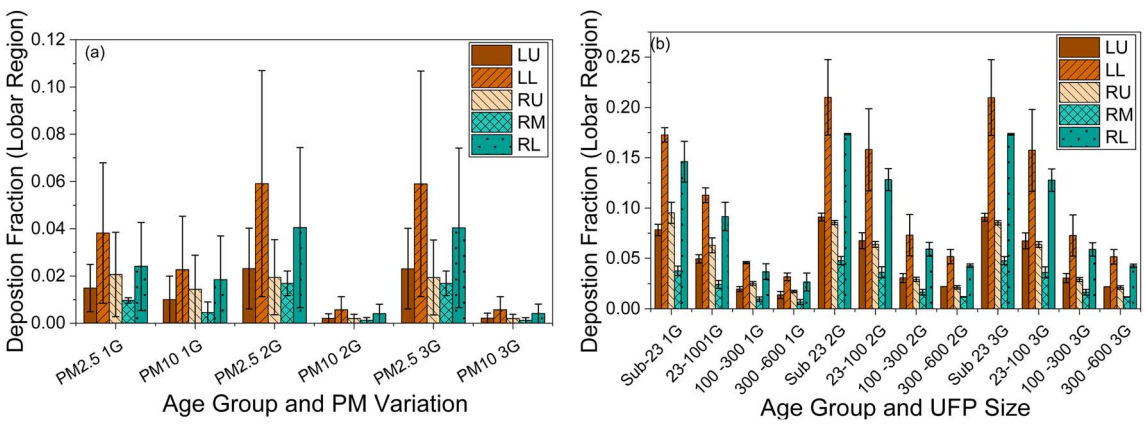

Fig. 4 Deposited fraction (DF) of $PM_{2.5}$, PM_{10}, and UFPs across different size ranges in various lung lobes for different age groups. (a) Deposition fraction of $PM_{2.5}$ and PM_{10}, and (b) deposition fraction of UFPs in four size ranges: (1) 23 nm, (2) 23 to 100 nm, (3) 100 to 300 nm, and (4) 300 to 600 nm. The deposition is shown for the right lower lobe (RL), right middle lobe (RM), right upper lobe (RU), left lower lobe (LL), and left upper lobe (LU), across three age groups: 1G (16–20 years), 2G (21–40 years), and 3G (41–60 years).

current in SMAW (from 50 A up to 125 A) leads to an apparent increase in PM deposition across all lobes for both PM_{10} and $PM_{2.5}$. LL and RL remain predominant areas of deposition at higher current among the lobes.

WAAM 18 V 65 A shows higher deposition in the lungs compared to the 25 V 125 A. $PM_{2.5}$ is more readily deposited in the lungs than PM_{10} for both welding methods and their respective parameters. Fig. S6 and S7 depict the number deposition of UFPs across four size ranges, sub-23 nm, 23–100 nm, 100–300 nm, and 300–600 nm, from SMAW and WAAM in different lung lobes under various operating conditions. The results indicate that, in all lung lobes, particles smaller than 100 nm deposit in greater numbers than those larger than 100 nm. Additionally, the older age group (41–60 years) experiences higher particle deposition across lung lobes compared to the younger group (16–20 years) (Fig. S6). For SMAW, an increase in current correlates with a rise in particle deposition in the lung lobes (Fig. S6). In WAAM, deposition is higher at 18 V 65 A compared to 25 V 125 A (Fig. S7).

3.2.4 Lung retention for $PM_{2.5}$ from SMAW and WAAM. The regional lung retention of welding fume particles, encompassing both deposition and clearance, was assessed using a one-week simulation comprising six exposure days of 8 hours each, followed by one day without exposure. This evaluation was conducted for the average $PM_{2.5}$ concentrations from various welding techniques, incorporating their respective parameters and particle densities, specifically for the 21–40 age group (Fig. S8). Deposition was generally greater in the tracheobronchial region compared to the alveolar region. However, the tracheobronchial region exhibited more efficient clearance mechanisms, leading to a rapid decline in retention during the non-exposure periods. In contrast, the alveolar region, characterised by slower clearance, showed a gradual accumulation of retained particles over time. At the end of the first and sixth work shifts for SMAW at 125 amperes, tracheobronchial retention was 0.06 and 0.045 μg cm^{-2}, respectively, while alveolar retention measured 1.3 and 8.02 μg. Following the one-week simulation (including one clearance day), retention levels decreased to 0.028 μg cm^{-2} in the tracheobronchial region and 8.01 μg in the alveolar region. The summarised results are presented here, while detailed retention profiles for different welding techniques and lifetime exposure scenarios (for 45 years) are provided in the SI (Fig. S8 and S9).

3.3 Health risk assessment

This study investigated the health risks faced by occupational workers during welding processes in an industrial workshop within an educational institution. It examined the exposure index, carcinogenic and non-carcinogenic risks, and the potential health impacts of UFPs, $PM_{2.5}$, and PM_{10} exposure. The findings revealed that SMAW at 125 amperes had the highest exposure index (15.4), significantly exceeding the levels observed during SMAW at 100 amperes (13.2). The lowest exposure index for SMAW was recorded at 50 amperes (3.6) and 75 amperes (6.7). These results indicate that the exposure index also increases as the current rating increases in SMAW. For WAAM, the emissions index was highest for 18 volts, 65 amperes (7.2), and minimum for 25 volts 125 amperes (5.02). These results emphasise that workers in industrial workshops using different welding techniques experience higher pollutant exposure, underscoring the need for targeted interventions to mitigate health risks in such environments. Carcinogenic risks were evaluated by calculating the ELCR, which ranged from 1.28×10^{-4} to 6.88×10^{-4} (Table S3). These values exceed the acceptable limits established by both the World Health Organization (WHO) and the US Environmental Protection Agency (USEPA). According to WHO (2013),[85] the acceptable ELCR range for humans is between 1×10^{-6} and 1×10^{-5}, while USEPA (2015)[65] sets a stricter limit of 1×10^{-6}. In this study, the mean ELCR for SMAW across all amperages was 3.4×10^{-4}, surpassing the WHO upper threshold by an order of magnitude and exceeding the USEPA guideline by two orders of magnitude. The highest recorded ELCR value (6.89×10^{-4}) for SMAW at 125 amperes exceeded the USEPA limit by up to two orders of magnitude. Even the lowest ELCR value (1.29×10^{-4}) observed at 50 amperes exceeded the USEPA acceptable threshold by two orders of magnitude, highlighting significant potential health risks. A comparison of ELCR values across different age groups indicates that younger individuals (16–20 years) are 25% (Table S3) more susceptible to cancer risk, as their ELCR values are significantly higher than those of older age groups (21 to 60 years). The higher ELCR observed in the 16–20 years age group is attributed to their lower body weight and inhalation rate, which serve as inverse functions in the calculation of SF and LADD used in the calculation of ELCR, within the standard USEPA risk assessment framework. The ELCR values reported in this study exceed those documented in previous research[61,63,64,69] on various emission sources, *e.g.*, kitchens. These findings highlight the substantial carcinogenic risks faced by occupational workers, particularly in industrial settings.

This study also calculated the Hazard Quotient (HQ) for both $PM_{2.5}$ and PM_{10} for different welding techniques used in industrial welding environments. An HQ > 1 indicates a potential health concern, while an HQ < 1 suggests no significant adverse health effects. The HQ values for $PM_{2.5}$ ranged from 20 to 88, while for PM_{10}, the values varied from 16 to 81 (Table S3). These findings suggest that most welding workshops exhibit pollutant concentrations exceeding the threshold. The highest HQ value of 88, recorded in a workshop, was attributed to Shielded Metal Arc Welding (SMAW) use at 125 amperes and the high intensity of welding activities. HQ values for $PM_{2.5}$ and PM_{10} exceeded the safety limit (HQ < 1) across all welding techniques and parameters, indicating the need for mitigation strategies to reduce inhalation risks.

Prolonged exposure to elevated PM levels in welding environments is associated with both immediate and long-term health effects, especially cardiovascular and respiratory diseases. According to WHO (2013),[85] $PM_{2.5}$ is responsible for approximately 8% of lung cancer deaths, 5% of cardiovascular diseases, and 3% of respiratory infection fatalities. Numerous studies[64,86,87] show a strong link between PM exposure and

mortality from cardiovascular and respiratory conditions. This study quantified attributable health risks using ER and AF metrics for all-cause, cardiopulmonary, and lung cancer mortality. The ER values for all-cause mortality ranged from 0.95 to 29.2 (Table S3), while AF values ranged from 0.49 to 0.97 (Table S2). These findings suggest a significant impact of PM exposure on workers performing welding in different industrial settings, which is very high compared to other studies (other emission sources).

For cardiopulmonary mortality due to $PM_{2.5}$ exposure, ER values ranged from 0.90 to 1.66, and AF values ranged from 0.41 to 0.62 for lung cancer mortality. ER values varied from 0.54 to 0.97, and AF values ranged from 0.35 to 0.48 for cardiopulmonary mortality (Table S3). These results indicate significantly higher health risks compared to previous studies, such as those in ref. 88 in Poland and ref. 62 in Nigeria, which reported lower ER and AF values for lung cancer and cardiopulmonary mortality.

3.4 Strengths and limitations of the study

This study's strengths include a detailed evaluation of welding emissions under controlled conditions, covering multiple welding techniques, parameters, and particle sizes, which enhances the reliability of the results. While respiratory deposition patterns align with prior modeling studies, we uniquely advance exposure assessment by systematically incorporating standardised input parameters—such as breathing rates, functional residual capacity, height, inhalation rate, activity levels, and particle characteristics based on established occupational and environmental standards. This methodical and standardised framework constitutes a novel and significant contribution to the exposure assessment of welding-related particulate matter.

Using precise, instrument-measured data, such as PM concentrations and UFP size distributions, ensures accuracy and minimises potential errors in estimates or model parameterisation. Additionally, incorporating real-world welding scenarios and considering factors like current, voltage, and feed rates provides a comprehensive understanding of exposure levels. A key strength is the focus on UFPs, for which information remains limited compared to the more extensively studied $PM_{2.5}$ and PM_{10}. These results reinforce recent calls in the literature for the comprehensive inclusion of ultrafine particles in workplace air quality guidelines. The notably high deposition of fine and ultrafine particles observed in this study highlights the critical need to develop and implement exposure limits and standards explicitly targeting these particle size fractions in occupational environments, thereby better safeguarding worker respiratory health. Raising awareness among workers and facility managers, along with enforcing the use of engineering controls and personal protective equipment (PPE), is essential to mitigating these risks. However, the analysis primarily focuses on idealised particles, assuming spherical shapes and uniform density, without accounting for the complex chemical composition of welding fumes. Future research should address these limitations by incorporating particle composition analysis, environmental variability, and clinical investigations into oxidative stress and inflammatory responses associated with welding fume exposure. Such studies would enhance the understanding of particle deposition in both the deep lung and proximal airways, providing a more comprehensive perspective on the health risks of welding emissions.

4. Conclusion

Assessing PM health risks is more effective through respiratory tract deposition rather than ambient exposure. This study analysed PM_{10}, $PM_{2.5}$, and UFP deposition in the head, TB, and P regions for SMAW, WAAM, and FSW welding in a central workshop. It examined dispersion patterns across three male age groups in an environment replicating real industrial settings. The study established correlations between deposition and welding parameters (current, voltage, feed rate, RPM), providing insights to optimise operating conditions while reducing human exposure. The results from the MPPD model indicated higher total DF for PM_{10} than for $PM_{2.5}$ and UFPs. $PM_{2.5}$ and PM_{10} primarily accumulated in the head region (35–90% and 80–99%, respectively), while UFPs showed the highest deposition in the pulmonary region (sub 23 nm: 53–83%, 23–100 nm: 28–63%, 100–600 nm: 28–70%). Overall, males of the 21–60 age group exhibited higher total deposition fraction across all particle sizes, except for PM_{10} in the teenage group (16–20). PM_{10} deposition was highest in the TB region (16–20 age group), peaking at 0.0137 μg (SMAW-125 amperes) and 0.00691 μg (WAAM-18 volts 65 amperes). $PM_{2.5}$ deposition in the TB region was highest for the 21–40 age group, peaking at 2.49×10^{-3} μg (SMAW-125 amperes) and 1.67×10^{-3} μg (WAAM-18 volts 65 amperes). UFP deposition from SMAW, WAAM, and FSW was higher for particles <100 nm compared to those in the 100–600 nm range. Lobar deposition analysis showed that UFP deposition exceeded $PM_{2.5}$ and PM_{10}, with the lower lobes receiving the highest deposition, and total deposition being greater in the left lung than the right. Excess lifetime cancer risk (1.28×10^{-4} to 6.88×10^{-4}) exceeded the USEPA recommended limit (1×10^{-6}) by two orders of magnitude. HQ values for $PM_{2.5}$ (20–88) and PM_{10} (16–81) exceeded one across all welding settings, indicating a high carcinogenic risk for workers. Authorities should implement measures to minimise human exposure to welding emissions in industrial settings by optimising ventilation systems and ensuring the use of appropriate protective equipment. Our findings also reveal significant gaps in current occupational exposure standards, which predominantly regulate respirable PM but overlook fine and ultrafine particles. This study provides quantitative deposition and risk data that can inform the development of updated guidelines and exposure limits, which are essential to better protect workers from the adverse health effects of particulate emissions in welding environments.

Author contributions

Rubal Dhiman: writing – original draft, methodology, investigation, formal analysis, data curation, conceptualisation.

Adarsh Prakash: investigation, review & editing, formal analysis. Subhrajyoti Saroj: investigation, formal analysis. Priyabrata Sahoo: review & editing, supervision, resources, methodology. Anirudha Ambekar: writing – review & editing, supervision, project administration, investigation, formal analysis. Sachin D. Kore: review & editing, supervision, resources, methodology. Thaseem Thajudeen: writing – review & editing, supervision, resources, project administration, funding acquisition, conceptualisation. Sarath K. Guttikunda: writing – review & editing, resources, methodology.

Conflicts of interest

The authors declare that they have no known competing financial interests or personal relationships that could have appeared to influence the work reported in this paper.

Data availability

All data generated or analyzed during this study are included in this published article and its supplementary information (SI). No additional datasets were created or used beyond those presented here. Supplementary information: details of Relative Risk (RR), Excess Risk (ER), and Attributable Fraction (AF); PM concentration data; PM deposition in the TB; deposition of PM in FSW, deposited mass and number from SMAW, WAAM in different lungs lobes, lungs retension doses for $PM_{2.5}$ from SMAW and WAAM. See DOI: **https://doi.org/10.1039/d5va00142k**.

Acknowledgements

Thaseem Thajudeen gratefully acknowledges the support from the Indian Institute of Technology Goa through the project 2018/TT/SG/006. The authors thank the Ministry of Education (MoE), Government of India, for financial support through the fellowships awarded to Rubal Dhiman, Adarsh Prakash, and Subhrajyoti Saroj, which enabled the successful execution of this research work at the Indian Institute of Technology Goa.

References

1 Y. S. Hedberg, Z. Wei, S. McCarrick, V. Romanovski, J. Theodore, E. M. Westin, R. Wagner, K. A. Persson, H. L. Karlsson and I. Odnevall Wallinder, Welding Fume Nanoparticles from Solid and Flux-Cored Wires: Solubility, Toxicity, and Role of Fluorides, *J. Hazard. Mater.*, 2021, **413**, 125273, DOI: **10.1016/j.jhazmat.2021.125273**.

2 J. B. Cortes, P. Sarazin, D. Dieme, J. Côté, C. Ouellet, N. El Majidi and M. Bouchard, Biomonitoring of Exposure to Multiple Metal Components in Urine, Hair and Nails of Apprentice Welders Performing Shielded Metal Arc Welding (SMAW), *Environ. Res.*, 2023, **239**(2), 117361, DOI: **10.1016/j.envres.2023.117361**.

3 IARC, *Welding, Molybdenum Trioxide, and Indium Tin Oxide*, 2017, vol. 118.

4 Y. Mehrifar, Z. Zamanian and H. Pirami, Respiratory Exposure to Toxic Gases and Metal Fumes Produced by Welding Processes and Pulmonary Function Tests, *Int. J. Occup. Environ. Med.*, 2019, **10**(1), 40–49, DOI: **10.15171/ijoem.2019.1540**.

5 R. E. Korczynski, Occupational Health Concerns in the Welding Industry, *Appl. Occup. Environ. Hyg.*, 2000, **15**(12), 936–945, DOI: **10.1080/104732200750051175**.

6 S. K. Guttikunda and R. Goel, Health Impacts of Particulate Pollution in a Megacity-Delhi, India, *Environ. Dev.*, 2013, **6**(1), 8–20, DOI: **10.1016/j.envdev.2012.12.002**.

7 B. Sjögren, M. Albin, K. Broberg, P. Gustavsson, H. Tinnerberg and G. Johanson, An Occupational Exposure Limit for Welding Fumes Is Urgently Needed, *Scand. J. Work, Environ. Health*, 2022, **48**(1), 1–3, DOI: **10.5271/sjweh.4002**.

8 J. Takahashi, H. Nakashima and N. Fujii, Fume Particle Size Distribution and Fume Generation Rate during Arc Welding of Cast Iron, *Ind. Health*, 2020, **58**(4), 325–334, DOI: **10.2486/indhealth.2019-0161**.

9 M. Keane, S. Stone and B. Chen, Welding Fumes from Stainless Steel Gas Metal Arc Processes Contain Multiple Manganese Chemical Species, *J. Environ. Monit.*, 2010, **12**(5), 1133–1140, DOI: **10.1039/b922840c**.

10 A. T. Zimmer, P. A. Baron and P. Biswas, The Influence of Operating Parameters on Number-Weighted Aerosol Size Distribution Generated from a Gas Metal Arc Welding Process, *J. Aerosol Sci.*, 2002, **33**(3), 519–531, DOI: **10.1016/S0021-8502(01)00189-6**.

11 K. Kirichenko, A. Zakharenko, K. Pikula, V. Chaika, Z. Markina, T. Orlova, S. Medvedev, G. Waissi, A. Kholodov, A. Tsatsakis and K. Golokhvast, Dependence of Welding Fume Particle Toxicity on Electrode Type and Current Intensity Assessed by Microalgae Growth Inhibition Test, *Environ. Res.*, 2019, **179**, 108818, DOI: **10.1016/j.envres.2019.108818**.

12 J. M. Antonini, A. Afshari, T. G. Meighan, W. McKinney, M. Jackson, D. Schwegler-Berry, D. A. Burns, R. F. LeBouf, B. T. Chen, M. Shoeb and P. C. Zeidler-Erdely, Aerosol Characterization and Pulmonary Responses in Rats after Short-Term Inhalation of Fumes Generated during Resistance Spot Welding of Galvanized Steel, *Toxicol. Rep.*, 2017, **4**, 123–133, DOI: **10.1016/j.toxrep.2017.02.004**.

13 M. M. Badami, R. Tohidi, V. Jalali Farahani and C. Sioutas, Size-Segregated Source Identification of Water-Soluble and Water-Insoluble Metals and Trace Elements of Coarse and Fine PM in Central Los Angeles, *Atmos. Environ.*, 2023, **310**(1994), 1–25, DOI: **10.1016/j.atmosenv.2023.119984**.

14 B. Berlinger, D. G. Ellingsen, M. Náray, G. Záray and Y. Thomassen, A Study of the Bio-Accessibility of Welding Fumes, *J. Environ. Monit.*, 2008, **10**(12), 1448–1453, DOI: **10.1039/b806631k**.

15 D. M. Brown, M. R. Wilson, W. MacNee, V. Stone and K. Donaldson, Size-Dependent Proinflammatory Effects of Ultrafine Polystyrene Particles: A Role for Surface Area and Oxidative Stress in the Enhanced Activity of Ultrafines,

Toxicol. Appl. Pharmacol., 2001, **175**(3), 191–199, DOI: 10.1006/taap.2001.9240.

16 K. Slezakova, E. de Oliveira Fernandes and M. d. C. Pereira, Assessment of Ultrafine Particles in Primary Schools: Emphasis on Different Indoor Microenvironments, *Environ. Pollut.*, 2019, **246**, 885–895, DOI: 10.1016/j.envpol.2018.12.073.

17 D. R. Johnson, Nanometer-Sized Emissions from Municipal Waste Incinerators: A Qualitative Risk Assessment, *J. Hazard. Mater.*, 2016, **320**, 67–79, DOI: 10.1016/j.jhazmat.2016.08.016.

18 R. X. Ward, T. B. Tilly, S. I. Mazhar, S. E. Robinson, A. Eiguren-Fernandez, J. Wang, T. Sabo-Attwood and C. Y. Wu, Mimicking the Human Respiratory System: Online in Vitro Cell Exposure for Toxicity Assessment of Welding Fume Aerosol, *J. Hazard. Mater.*, 2020, **395**, 122687, DOI: 10.1016/j.jhazmat.2020.122687.

19 N. Manojkumar, B. Srimuruganandam and S. M. Shiva Nagendra, Application of Multiple-Path Particle Dosimetry Model for Quantifying Age Specified Deposition of Particulate Matter in Human Airway, *Ecotoxicol. Environ. Saf.*, 2019, **168**, 241–248, DOI: 10.1016/j.ecoenv.2018.10.091.

20 Since January 2020 Elsevier Has Created a COVID-19 Resource Centre with Free Information in English and Mandarin on the Novel Coronavirus COVID-19. The COVID-19 Resource Centre Is Hosted on Elsevier Connect, the Company's Public News and Information, 2020, January.

21 J. Zheng, Z. Qiu, H. O. Gao and B. Li, Commuter PM Exposure and Estimated Life-Expectancy Loss across Multiple Transportation Modes in Xi'an, China, *Ecotoxicol. Environ. Saf.*, 2021, **214**, 112117, DOI: 10.1016/j.ecoenv.2021.112117.

22 S. Khan, B. R. Gurjar and V. Sahu, Deposition Modeling of Ambient Particulate Matter in the Human Respiratory Tract, *Atmos. Pollut. Res.*, 2022, **13**(10), 101565, DOI: 10.1016/j.apr.2022.101565.

23 R. J. Delfino, C. Sioutas and S. Malik, Potential Role of Ultrafine Particles in Associations between Airborne Particle Mass and Cardiovascular Health, *Environ. Health Perspect.*, 2005, **113**(8), 934–946, DOI: 10.1289/ehp.7938.

24 D. E. Schraufnagel, The Health Effects of Ultrafine Particles, *Exp. Mol. Med.*, 2020, **52**(3), 311–317, DOI: 10.1038/s12276-020-0403-3.

25 Y. J. Kim, I. G. Song, K. N. Kim, M. S. Kim, S. H. Chung, Y. S. Choi and C. W. Bae, Maternal Exposure to Particulate Matter during Pregnancy and Adverse Birth Outcomes in the Republic of Korea, *Int. J. Environ. Res. Public Health*, 2019, **16**(4), 1–10, DOI: 10.3390/ijerph16040633.

26 M. Geiser, B. Rothen-Rutishauser, N. Kapp, S. Schürch, W. Kreyling, H. Schulz, M. Semmler, V. Im Hof, J. Heyder and P. Gehr, Ultrafine Particles Cross Cellular Membranes by Nonphagocytic Mechanisms in Lungs and in Cultured Cells, *Environ. Health Perspect.*, 2005, **113**(11), 1555–1560, DOI: 10.1289/ehp.8006.

27 L. M. T. Luong, D. Phung, P. D. Sly, L. Morawska and P. K. Thai, The Association between Particulate Air Pollution and Respiratory Admissions among Young Children in Hanoi, Vietnam, *Sci. Total Environ.*, 2017, **578**, 249–255, DOI: 10.1016/j.scitotenv.2016.08.012.

28 A. J. Cohen, M. Brauer, R. Burnett, H. R. Anderson, J. Frostad, K. Estep, K. Balakrishnan, B. Brunekreef, L. Dandona, R. Dandona, V. Feigin, G. Freedman, B. Hubbell, A. Jobling, H. Kan, L. Knibbs, Y. Liu, R. Martin, L. Morawska, C. A. Pope, H. Shin, K. Straif, G. Shaddick, M. Thomas, R. van Dingenen, A. van Donkelaar, T. Vos, C. J. L. Murray and M. H. Forouzanfar, Estimates and 25-Year Trends of the Global Burden of Disease Attributable to Ambient Air Pollution: An Analysis of Data from the Global Burden of Diseases Study 2015, *Lancet*, 2017, **389**(10082), 1907–1918, DOI: 10.1016/S0140-6736(17)30505-6.

29 J. Madureira, K. Slezakova, A. I. Silva, B. Lage, A. Mendes, L. Aguiar, M. C. Pereira, J. P. Teixeira and C. Costa, Assessment of Indoor Air Exposure at Residential Homes: Inhalation Dose and Lung Deposition of PM_{10}, $PM_{2.5}$ and Ultrafine Particles among Newborn Children and Their Mothers, *Sci. Total Environ.*, 2020, **717**, 137293, DOI: 10.1016/j.scitotenv.2020.137293.

30 S. A. "Ainaa" Idris, M. M. Hanafiah, M. Ismail, S. Abdullah and M. F. Khan, Laboratory Air Quality and Microbiological Contamination in a University Building, *Arabian J. Geosci.*, 2020, **13**(13), 580, DOI: 10.1007/s12517-020-05564-8.

31 S. McCarrick, Z. Wei, N. Moelijker, R. Derr, K. A. Persson, G. Hendriks, I. Odnevall Wallinder, Y. Hedberg and H. L. Karlsson, High Variability in Toxicity of Welding Fume Nanoparticles from Stainless Steel in Lung Cells and Reporter Cell Lines: The Role of Particle Reactivity and Solubility, *Nanotoxicology*, 2019, **13**(10), 1293–1309, DOI: 10.1080/17435390.2019.1650972.

32 M. A. Suliman, A. Wahab, M. A. M. Dari, M. S. b. Hamid, M. I. A. Wahab, K. Subari and S. Irum, A Study of Welder Age on Welding Quality for Oil and Gas Offshore Structural Fabrication Project, *Pakistan Journal of Life and Social Sciences*, 2024, **22**(2), 3030–3047, DOI: 10.57239/pjlss-2024-22.2.00223.

33 M. G. Riccelli, M. Goldoni, D. Poli, P. Mozzoni, D. Cavallo and M. Corradi, Welding Fumes, a Risk Factor for Lung Diseases, *Int. J. Environ. Res. Public Health*, 2020, **17**(7), 2552, DOI: 10.3390/ijerph17072552.

34 A. Khan, L. Davulienė, S. Šemčuk, K. Kandrotaitė, A. Minderytė, M. Davtalab, I. Uogintė, M. Skapas, V. Dudoitis and S. Byčenkienė, Integrated Personal Exposure and Deposition of Black Carbon on Human Lungs, *Air Qual., Atmos. Health*, 2024, **17**(1), 35–50, DOI: 10.1007/s11869-023-01428-8.

35 J. Rissler, A. Gudmundsson, H. Nicklasson, E. Swietlicki, P. Wollmer and J. Löndahl, Deposition Efficiency of Inhaled Particles (15-5000 Nm) Related to Breathing Pattern and Lung Function: An Experimental Study in Healthy Children and Adults, *Part. Fibre Toxicol.*, 2017, **14**(1), 1–12, DOI: 10.1186/s12989-017-0190-8.

36 I. Kolokolnikov, E. Nepomnyashchaya and E. Velichko, Static Light Scattering for Determination of Physical Parameters of

Macro- and Nanoparticles, *J. Phys.: Conf. Ser.*, 2019, **1410**(1), 012168, DOI: 10.1088/1742-6596/1410/1/012168.

37 R. Dhiman, A. Prakash, S. Saroj, P. Sahoo, A. Ambekar, S. D. Kore, T. Thajudeen and S. K. Guttikunda, Comprehensive Analysis of the Fine and Ultrafine Particulate Emissions from Various Welding Sources in an Industrial Environment, *Atmos. Pollut. Res.*, 2025, **16**(12), 102666, DOI: 10.1016/j.apr.2025.102666.

38 A. Prakash, R. Dhiman, A. Ambekar, T. Thajudeen and S. Dnyandeo, Investigating the Effect of Varying Powder Size Range on Particulate Matter Emission and Mechanical Properties of in Situ Micropowder Alloyed WAAM Depositions, *Weld. World*, 2025, DOI: 10.1007/s40194-024-01922-2.

39 J. Sajedifar, A. H. Kokabi, S. F. Dehghan, A. Mehri, K. Azam and F. Golbabaei, Evaluation of Operational Parameters Role on the Emission of Fumes, *Ind. Health*, 2018, **56**(3), 198–206, DOI: 10.2486/indhealth.2017-0155.

40 N. Serfozo and M. Lazaridis, Estimation of Particle Emission Rates and Calculation of Human Dose from Arc Welding and Cutting of Stainless Steel in a Simulated Confined Workspace, *Aerosol Science and Engineering*, 2023, **7**(4), 474–487, DOI: 10.1007/s41810-023-00192-7.

41 S. Wang, Z. Gao, G. Wu and X. Mao, Titanium Microalloying of Steel: A Review of Its Effects on Processing, Microstructure and Mechanical Properties, *Int. J. Miner., Metall. Mater.*, 2022, **29**(4), 645–661, DOI: 10.1007/s12613-021-2399-7.

42 A. Mostafapour, A. Ebrahimpour and T. Saeid, Identification of Retained Austenite, Ferrite, Bainite and Martensite in the Microstructure of TRIP Steel, *Int. J. ISSI*, 2016, **13**(2), 1–6.

43 S. Saroj, R. Dhiman, A. Prakash, P. Sahoo and A. Ambekar, Mitigation of Internal Weld Defects and Ultra-Fine Particulate Emission by Induction Preheating in Friction Stir Welding, *Weld. World*, 2025, DOI: 10.1007/s40194-025-02146-8.

44 A. Prakash, R. Dhiman, A. Ambekar, T. Thajudeen and S. D. Kore, Investigations into Metallurgical, Mechanical, and Particulate Matter Emissions in in Situ Micropowder Alloyed Wire Arc Additive Manufacturing Process, *Weld. Int.*, 2024, 1–16, DOI: 10.1080/09507116.2024.2442481.

45 A. Goel, S. Izhar and T. Gupta, Study of Environmental Particle Levels, Its Effects on Lung Deposition and Relationship with Human Behaviour, *Energy Environ. Sustainability*, 2018, 77–91, DOI: 10.1007/978-981-10-7332-8_4.

46 H. Lv, H. Li, Z. Qiu, F. Zhang and J. Song, Assessment of Pedestrian Exposure and Deposition of PM_{10}, $PM_{2.5}$ and Ultrafine Particles at an Urban Roadside: A Case Study of Xi'an, China, *Atmos. Pollut. Res.*, 2021, **12**(4), 112–121, DOI: 10.1016/j.apr.2021.02.018.

47 A. Nong, M. D. Taylor, H. J. Clewell, D. C. Dorman and M. E. Andersen, Manganese Tissue Dosimetry in Rats and Monkeys: Accounting for Dietary and Inhaled Mn with Physiologically Based Pharmacokinetic Modeling, *Toxicol. Sci.*, 2009, **108**(1), 22–34, DOI: 10.1093/toxsci/kfn264.

48 W. Hofmann, Modelling Inhaled Particle Deposition in the Human Lung-A Review, *J. Aerosol Sci.*, 2011, **42**(10), 693–724, DOI: 10.1016/j.jaerosci.2011.05.007.

49 K. Pillay, W. H. Finlay and A. R. Martin, Understanding Regional Aerosol Deposition in Pediatric Airways during Oral Breathing: Insights from Computational Modeling, *J. Aerosol Sci.*, 2024, **182**, 106438, DOI: 10.1016/j.jaerosci.2024.106438.

50 L. Ma, Y. Zhang, Z. Lin, Y. Zhou, C. Yan, Y. Zhang, W. Zhou, W. Ma, C. Hua, X. Li, C. Deng, Y. Qi, L. Dada, H. Li, F. Bianchi, T. Petäjä, J. Kangasluoma, J. Jiang, S. Liu, T. Hussein, M. Kulmala and Y. Liu, Deposition Potential of 0.003–10 Mm Ambient Particles in the Humidified Human Respiratory Tract: Contribution of New Particle Formation Events in Beijing, *Ecotoxicol. Environ. Saf.*, 2022, **243**, 114023, DOI: 10.1016/j.ecoenv.2022.114023.

51 J. S. Brown, T. Gordon, O. Price and B. Asgharian, Thoracic and Respirable Particle Definitions for Human Health Risk Assessment, *Part. Fibre Toxicol.*, 2013, **10**(1), 1–12, DOI: 10.1186/1743-8977-10-12.

52 W. Yin, J. Hou, T. Xu, J. Cheng, X. Wang, S. Jiao, L. Wang, C. Huang, Y. Zhang and J. Yuan, Association of Individual-Level Concentrations and Human Respiratory Tract Deposited Doses of Fine Particulate Matter with Alternation in Blood Pressure, *Environ. Pollut.*, 2017, **230**, 621–631, DOI: 10.1016/j.envpol.2017.07.006.

53 S. Heydarian, M. Mahjoob, A. Gholami, S. Veysi and M. Mohammadi, Prevalencia de La Deficiencia de La Visión Del Color Entre Los Soldadores Con Arco Eléctrico, *J. Optom.*, 2017, **10**(2), 130–134, DOI: 10.1016/j.optom.2015.12.007.

54 R. Greenwald, M. J. Hayat, E. Dons, L. Giles, R. Villar, D. G. Jakovljevic and N. Good, Estimating Minute Ventilation and Air Pollution Inhaled Dose Using Heart Rate, Breath Frequency, Age, Sex and Forced Vital Capacity: A Pooled-Data Analysis, *PLoS One*, 2019, **14**(7), 1–18, DOI: 10.1371/journal.pone.0218673.

55 Y. Ostchega, K. S. Porter, J. Hughes, C. F. Dillon and T. Nwankwo, Resting Pulse Rate Reference Data for Children, Adolescents, and Adults: United States, 1999-2008, *National Health Statistics Reports*, 2011, (41), 1999–2008.

56 S. Kugler, A. Nagy, J. Osán, L. Péter, V. Groma, S. Pollastri and A. Czitrovszky, Characterization of the Ultrafine and Fine Particles Formed during Laser Cladding with the Inconel 718 Metal Powder by Means of X-Ray Spectroscopic Techniques, *Spectrochim. Acta, Part B*, 2021, **177**, 106110, DOI: 10.1016/j.sab.2021.106110.

57 W. Jiang, Y. Xu, M. Zhang and S. Ma, Quantitative Analysis of the Factors That Influence Welding Fume Exposure via ART Modelling, *Saf. Health Work*, 2025, DOI: 10.1016/j.shaw.2025.06.004.

58 S. J. Mbazima, Health Risk Assessment of Particulate Matter 2.5 in an Academic Metallurgy Workshop, *Indoor Air*, 2022, **32**(9), 1–13, DOI: 10.1111/ina.13111.

59 Golder Associates, *Exposure Assessment and Risk Characterisation to Inform Recommendations for Updating*

Ambient Air Quality Standards for $PM_{2.5}$, PM_{10}, O_3, NO_2, SO_2, 2013.

60 K. F. R. Liu, K. Yeh, M.-J. Hung, C.-W. Chen and Y.-S. Shen, Health Risk Analysis of Indoor Air Pollution, *Int. J. Environ. Sci. Dev.*, 2015, **6**(6), 464–468, DOI: 10.7763/ijesd.2015.v6.638.

61 E. Konduracka and P. Rostoff, Links between Chronic Exposure to Outdoor Air Pollution and Cardiovascular Diseases: A Review, *Environ. Chem. Lett.*, 2022, **20**(5), 2971–2988, DOI: 10.1007/s10311-022-01450-9.

62 E. L. Odekanle, O. O. Sonibare, O. J. Odejobi, B. S. Fakinle and F. A. Akeredolu, Air Emissions and Health Risk Assessment around Abattoir Facility, *Heliyon*, 2020, **6**(7), e04365, DOI: 10.1016/j.heliyon.2020.e04365.

63 H. Kim, K. Kang and T. Kim, Measurement of Particulate Matter ($PM_{2.5}$) and Health Risk Assessment of Cooking-Generated Particles in the Kitchen and Living Rooms of Apartment Houses, *Sustain*, 2018, **10**(3), DOI: 10.3390/su10030843.

64 E. Chalvatzaki, S. E. Chatoutsidou, H. Lehtomäki, S. M. Almeida, K. Eleftheriadis, O. Hänninen and M. Lazaridis, Characterization of Human Health Risks from Particulate Air Pollution in Selected European Cities, *Atmosphere*, 2019, **10**(2), 1–16, DOI: 10.3390/ATMOS10020096.

65 US EPA, *US EPA Integrated Risk Information System (IRIS)*, United States Environmental Protection Agency, 2015, pp. 2–3.

66 I. Engelbrecht, S. Horn, C. J. Badenhorst and J. L. du Plessis, Beyond the Clock: Revisiting Occupational Exposure Limits (OELs) for Unusual Work Schedules in the South African Mining Industry, *Saf. Sci.*, 2024, **176**, 106542, DOI: 10.1016/j.ssci.2024.106542.

67 M. Waters, L. McKernan, A. Maier, M. Jayjock, V. Schaeffer and L. Brosseau, Exposure Estimation and Interpretation of Occupational Risk: Enhanced Information for the Occupational Risk Manager, *J. Occup. Environ. Hyg.*, 2015, **12**, S99–S111, DOI: 10.1080/15459624.2015.1084421.

68 EPA, Body Weight Studies, in *Exposure Factors Handbook*, 2011, ch. 8, pp. 1–56.

69 G. Heydari, F. Taghizdeh, M. Fazlzadeh, A. J. Jafari, Z. Asadgol, E. A. Mehrizi, M. Moradi and H. Arfaeinia, Levels and Health Risk Assessments of Particulate Matters ($PM_{2.5}$ and PM_{10}) in Indoor/Outdoor Air of Waterpipe Cafés in Tehran, Iran, *Environ. Sci. Pollut. Res.*, 2019, **26**(7), 7205–7215, DOI: 10.1007/s11356-019-04202-5.

70 M. K. Sidhu, K. Ravindra, S. Mor and S. John, Household Air Pollution from Various Types of Rural Kitchens and Its Exposure Assessment, *Sci. Total Environ.*, 2017, **586**, 419–429, DOI: 10.1016/j.scitotenv.2017.01.051.

71 World Health Organization, *WHO Global Air Quality Guidelines: Particulate Matter ($PM_{2.5}$ and PM_{10}), Ozone, Nitrogen Dioxide, Sulfur Dioxide and Carbon Monoxide*, Geneva, 2021, pp. 1–360.

72 EPA, *Risk Assessment Guidance for Superfund. Volume I: Human Health Evaluation Manual (Part A)*, 1989, vol. I, p. 289, EPA/540/1-89/002.

73 A. Prüss-Üstün, C. Mathers, C. Corvalan and A. Woodward, *Introduction and Methods: Assessing the Environmental Burden of Disease at National and Local Levels*, 2003.

74 D. Lizonova, A. Nagarkar, P. Demokritou and G. A. Kelesidis, Effective Density of Inhaled Environmental and Engineered Nanoparticles and Its Impact on the Lung Deposition and Dosimetry, *Part. Fibre Toxicol.*, 2024, **21**(1), 1–11, DOI: 10.1186/s12989-024-00567-9.

75 L. Famiyeh, C. Jia, K. Chen, Y. T. Tang, D. Ji, J. He and Q. Guo, Size Distribution and Lung-Deposition of Ambient Particulate Matter Oxidative Potential: A Contrast between Dithiothreitol and Ascorbic Acid Assays, *Environ. Pollut.*, 2023, **336**, 122437, DOI: 10.1016/j.envpol.2023.122437.

76 M. S. Islam, P. Larpruenrudee, S. I. Hossain, M. Rahimi-Gorji, Y. Gu, S. C. Saha and G. Paul, Polydisperse Aerosol Transport and Deposition in Upper Airways of Age-Specific Lung, *Int. J. Environ. Res. Public Health*, 2021, **18**(12), DOI: 10.3390/ijerph18126239.

77 Y. Li, H. Cui, L. Chen, M. Fan, J. Cai, J. Guo, C. U. Yurteri, X. Si, S. Liu, F. Xie and J. Xie, Modeled Respiratory Tract Deposition of Smoke Aerosol from Conventional Cigarettes, Electronic Cigarettes and Heat-Not-Burn Products, *Aerosol Air Qual. Res.*, 2021, **21**(5), DOI: 10.4209/aaqr.200241.

78 S. N. Behera, R. Betha, X. Huang and R. Balasubramanian, Characterization and Estimation of Human Airway Deposition of Size-Resolved Particulate-Bound Trace Elements during a Recent Haze Episode in Southeast Asia, *Environ. Sci. Pollut. Res.*, 2015, **22**(6), 4265–4280, DOI: 10.1007/s11356-014-3645-6.

79 B. Srimuruganandam, Quantification of Size Segregated Particulate Matter Deposition in Human Airways, *Journal of Advanced Research in Alternative Energy, Environment and Ecology*, 2018, **05**(04), 15–22, DOI: 10.24321/2455.3093.201803.

80 S. Y. Yang, J. M. Lin, L. H. Young and C. W. Chang, Mass-Size Distribution and Concentration of Metals from Personal Exposure to Arc Welding Fume in Pipeline Construction: A Case Report, *Ind. Health*, 2018, **56**(4), 356–363, DOI: 10.2486/indhealth.2017-0197.

81 A. R. Lambert, P. O. Shaughnessy, M. H. Tawhai, E. A. Hoffman and C. Lin, *Asymmetry*, 2011, **45**(1), 11–25, DOI: 10.1080/02786826.2010.517578.Regional.

82 P. C. Clarà, F. R. Jerez, J. B. Ramírez and C. M. González, Deposition and Clinical Impact of Inhaled Particles in the Lung, *Archivos de Bronconeumología*, 2023, **59**(6), 377–382, DOI: 10.1016/j.arbres.2023.01.016.

83 Y. A. Cipoli, L. Furst, M. Feliciano and C. Alves, Respiratory Deposition Dose of - $PM_{2.5}$ and - PM_{10} during Night and Day Periods at an Urban Environment, *Air Qual., Atmos. Health*, 2023, **16**(11), 2269–2283, DOI: 10.1007/s11869-023-01405-1.

84 S. Mahalingam and R. Narayanan, Influence of Body Mass Index on $PM_{2.5}$ Deposition in Respiratory Tract during Urban Commuting, *Air Qual., Atmos. Health*, 2024, 1983–1996, DOI: 10.1007/s11869-024-01558-7.

85 B. Festy, *Review of Evidence on Health Aspects of Air Pollution - REVIHAAP Project*, World Health Organization Regional Office for Europe, 2013.
86 N. Vaze, L. Calderon, I. Tsiodra, N. Mihalopoulos, C. N. Serhan, B. D. Levy and P. Demokritou, Assessment of the Physicochemical Properties of Ultrafine Particles (UFP) from Vehicular Emissions in a Commercial Parking Garage: Potential Health Implications, *Toxics*, 2024, **12**(11), DOI: **10.3390/toxics12110833**.
87 F. J. Kelly and J. C. Fussell, Size, Source and Chemical Composition as Determinants of Toxicity Attributable to Ambient Particulate Matter, *Atmos. Environ.*, 2012, **60**, 504–526, DOI: **10.1016/j.atmosenv.2012.06.039**.
88 A. J. Badyda, J. Grellier and P. Dąbrowiecki, Ambient $PM_{2.5}$ Exposure and Mortality Due to Lung Cancer and Cardiopulmonary Diseases in Polish Cities, *Adv. Exp. Med. Biol.*, 2017, **944**, 9–17, DOI: **10.1007/5584_2016_55**.